

Intention-Conditioned Flow Occupancy Models

Chongyi Zheng¹ Seohong Park² Sergey Levine² Benjamin Eysenbach¹
¹Princeton University ²University of California, Berkeley
chongyiz@princeton.edu

Abstract

Large-scale pre-training has fundamentally changed how machine learning research is done today: large foundation models are trained once, and then can be used by anyone in the community (including those without data or compute resources to train a model from scratch) to adapt and fine-tune to specific tasks. Applying this same framework to reinforcement learning (RL) is appealing because it offers compelling avenues for addressing core challenges in RL, including sample efficiency and robustness. However, there remains a fundamental challenge to pre-train large models in the context of RL: actions have long-term dependencies, so training a foundation model that reasons across *time* is important. Recent advances in generative AI have provided new tools for modeling highly complex distributions. In this paper, we build a probabilistic model to predict which states an agent will visit in the temporally distant future (i.e., an occupancy measure) using flow matching. As large datasets are often constructed by many distinct users performing distinct tasks, we include in our model a latent variable capturing the user intention. This intention increases the expressivity of our model, and enables adaptation with generalized policy improvement. We call our proposed method **intention-conditioned flow occupancy models (InFOM)**. Comparing with alternative methods for pre-training, our experiments on 36 state-based and 4 image-based benchmark tasks demonstrate that the proposed method achieves $1.8\times$ median improvement in returns and increases success rates by 36%.

Website: <https://chongyi-zheng.github.io/infom>

Code: <https://github.com/chongyi-zheng/infom>

1 Introduction

Many of the recent celebrated successes of machine learning have been enabled by training large foundation models on vast datasets, and then adapting those models to downstream tasks. Examples include today’s chatbots (e.g., Gemini [108] and ChatGPT [1]) and generalist robotic systems (e.g., π_0 [10] and Octo [109]). This pre-training-fine-tuning paradigm has been wildly successful in fields ranging from computer vision to natural language processing [22, 15, 116, 127, 91, 41, 78, 66], yet harnessing it in the context of reinforcement learning (RL) remains an open problem. What fundamentally makes the RL problem difficult is reasoning about time and intention—an effective RL agent must reason about the long-term effect of actions taken now, and must recognize that the data observed are often collected by distinct users

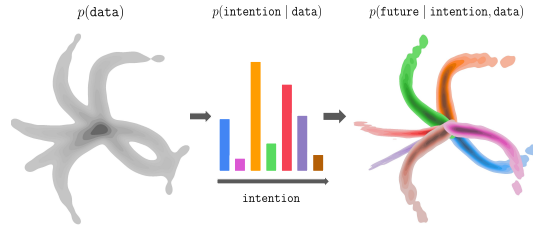


Figure 1: **InFOM** is a latent variable model for pre-training and fine-tuning in reinforcement learning. (Left) The datasets are collected by users performing distinct tasks. (Center) We encode intentions by maximizing an evidence lower bound of data likelihood, (Right) enabling intention-aware future prediction using flow matching. See Sec. 4 for details.

performing multiple tasks. However, current attempts to build foundation models for RL often neglect these two important bits, often focusing on predicting the actions in the pre-training dataset instead [109, 79, 120].

The closest attempts to building RL algorithms that capture temporal bits are those based on world models [23, 37, 72] and those based on occupancy models [52, 11, 129, 29].¹ World models can achieve great performance in sample efficiency [50] and generalize to diverse tasks [37, 72], although their capacity to perform long-horizon reasoning remains limited because of compounding errors [104, 50, 60]. Occupancy models [21] and variants that enable scaling to high-dimensional tasks can also achieve great performance in predicting future events [100, 8, 129, 130, 29], but are typically hard to train and ignore user intentions. Recent advances in generative AI (e.g., flow-matching [64, 63, 65] and diffusion [46, 102] models) enable modeling complex distributions taking various inputs, providing new tools for constructing occupancy models that depend on intentions.

In this paper, we propose a framework (Fig. 1) for pre-training in RL that simultaneously learns a probabilistic model to capture bits about time and intention. Building upon prior work on variational inference [57, 5] and successor representations [52, 113, 9, 129, 29], we learn latent variable models of temporally distant future states, enabling intention-aware prediction. Building upon prior work on generative modeling, we use an expressive flow matching method [29] to train occupancy models, enabling highly flexible modeling of occupancy measures. We call the resulting algorithm **intention-conditioned flow occupancy models (InFOM)**. Experiments on 36 state-based and 4 image-based benchmark tasks show that InFOM outperforms alternative methods for pre-training and fine-tuning by $1.8\times$ median improvement in returns and 36% improvement in success rates. Additional experiments demonstrate that our latent variable model is simple and performant in inferring intentions (Sec. 5.2) and enabling fast downstream adaptation (Sec. 5.4).

2 Related work

Offline unsupervised RL. The goal of offline unsupervised RL is to pre-train policies, value functions, or models from an unlabeled (reward-free) dataset to enable efficient learning of downstream tasks. Prior work has proposed diverse offline unsupervised RL approaches based on unsupervised skill learning [113, 31, 84, 55, 47], offline goal-conditioned RL [26, 28, 117, 83, 129, 81], and model-based RL [72, 71]. Among these categories, our method is conceptually related to offline unsupervised skill learning approaches [84, 114], which also learns a model that predicts intention. However, our approach differs in that it does not learn multiple skills during pre-training. In that we also learn a set of latent intentions that capture diverse behavioral modes in the dataset. Our work is complementary to a large body of prior work on using behavioral cloning for pretraining [79, 109], demonstrating that there are significant additional gains in performance that can be achieved by modeling intentions and occupancy measures simultaneously.

Unsupervised representation learning for RL. Another way to leverage an unlabeled offline dataset is to learn representations that facilitate subsequent downstream task learning. Some works adapt existing representation learning techniques from computer vision, such as contrastive learning [42, 80, 75] and masked autoencoding [41, 124]. Others design specific methods for RL, including self-predictive representations [98, 77] and temporal distance learning [99, 67, 70]. Those learned representations are typically used as inputs for policy and value networks. The key challenge with these representation learning methods is that it is often [61], though not always [128], unclear whether the learned representations will facilitate policy adaptation. In our experiments, we demonstrate that learning occupancy models enables faster policy learning.

RL with generative models. Modern generative models have been widely adopted to solve RL problems. Prior work has employed autoregressive models [119], iterative generative models (e.g., denoising diffusion [101, 46] and flow matching [65, 63, 64]), or autoencoders [57] to model trajectories [20, 51, 49, 2], environment dynamics [23, 6], skills [3, 87, 31], and policies [122, 39, 85]. We employ a state-of-the-art flow-matching objective [29] to model discounted state occupancy measures.

Successor representations and successor features. Prior work has used successor representations [21] and successor features [9] for transfer learning [9, 8, 12, 76, 54], unsupervised

¹We will use “successor representations,” “occupancy measures,” and “occupancy models” interchangeably.

RL [68, 38, 34, 114, 84, 86, 19, 130, 48, 132], and goal-conditioned RL [27, 28, 129]. Our method is closely related to prior methods that learn successor representations with generative models [52, 110, 112, 29]. In particular, the most closely related to ours is the prior work by Farebrother et al. [29], which also uses flow-matching to model the occupancy measures and partly employs the generalized policy improvement (GPI) for policy extraction. Unlike Farebrother et al. [29], which uses forward-backward representations to capture behavioral intentions and perform GPI over a finite set of intentions, our method employs a latent variable model to learn intentions (Sec. 4.2) and uses an expectile loss to perform implicit GPI (Sec. 4.4). We empirically show that these choices lead to higher returns and success rates (Sec. 5.1, Sec. 5.3).

3 Preliminaries

Value functions and occupancy measures. We consider a Markov decision process (MDP) [103] defined by a state space \mathcal{S} , an action space \mathcal{A} , an initial state distribution $\rho \in \Delta(\mathcal{S})$, a reward function $r : \mathcal{S} \rightarrow \mathbb{R}$, a discount factor $\gamma \in [0, 1)$, and a transition distribution $p : \mathcal{S} \times \mathcal{A} \rightarrow \Delta(\mathcal{S})$, where $\Delta(\cdot)$ denotes the set of all possible probability distributions over a space. We will use h to denote a time step in the MDP and assume the reward function only depends on the state at the current time step $r_h \triangleq r(s_h)$ without loss of generality [112, 31, 110]. The goal of RL is to learn a policy $\pi : \mathcal{S} \rightarrow \Delta(\mathcal{A})$ that maximizes the expected discounted return $J(\pi) = \mathbb{E}_{\tau \sim \pi(\tau)} [\sum_{h=0}^{\infty} \gamma^h r_h]$, where τ is a trajectory sampled by the policy. We will use $\beta : \mathcal{S} \rightarrow \Delta(\mathcal{A})$ to denote the behavioral policy. Given a policy π , we measure the expected discounted return starting from a state-action pair (s, a) and a state s as the (unnormalized) Q-function and the value function, respectively:

$$Q^\pi(s, a) = \mathbb{E}_{\tau \sim \pi(\tau)} \left[\sum_{h=0}^{\infty} \gamma^h r_h \mid s_0 = s, a_0 = a \right], \quad V^\pi(s) = \mathbb{E}_{a \sim \pi(a|s)} [Q^\pi(s, a)].$$

In Appendix A.1, we briefly review the actor-critic framework in RL.

Alternatively, one can summarize the stochasticity over trajectories into the *discounted state occupancy measure* [21, 28, 52, 113, 129, 74, 11] that quantifies the discounted visitation frequency of different states under the policy π . Using $p_h^\pi(s_f | s, a)$ to denote the probability density of reaching state s_f at exactly h steps in the future, starting at the state-action pair (s, a) and then following policy π , we define the discounted state occupancy measure as

$$p_\gamma^\pi(s_f | s, a) = (1 - \gamma) \sum_{h=0}^{\infty} \gamma^h p_h^\pi(s_f | s, a). \quad (1)$$

Prior work [21, 52, 113, 129] has shown that the discounted state occupancy measure follows a Bellman equation backing up the probability density at the current time step and the future time steps:

$$p_\gamma^\pi(s_f | s, a) = (1 - \gamma) \delta_s(s_f) + \gamma \mathbb{E}_{\substack{s' \sim p(s'|s, a) \\ a' \sim \pi(a'|s')}} [p_\gamma^\pi(s_f | s', a')], \quad (2)$$

where $\delta_s(\cdot)$ denotes the Dirac delta measure centered at s .² The discounted state occupancy measure allows us to rewrite the Q-function as a linear function of rewards [9, 113, 129, 100]:

$$Q^\pi(s, a) = \frac{1}{1 - \gamma} \mathbb{E}_{s_f \sim p_\gamma^\pi(s_f | s, a)} [r(s_f)]. \quad (3)$$

The alternative (dual [100]) definition of Q-function (Eq. 3) allows us to cast the policy evaluation step as first learning a generative model $p_\gamma(s_f | s, a)$ to simulate the discounted state occupancy measure of π^k and then regressing the estimator Q towards the average reward at states sampled from p_γ [115, 112, 110, 129]. See Sec. 4.4 for detailed formulation.

Flow matching and TD flows. Flow matching [63–65, 4] refers to a family of generative models based on ordinary differential equations (ODEs), which are close cousins of denoising diffusion models [101, 102, 46], which instead solve a stochastic differential equation (SDE). The deterministic nature of ODEs equips flow-matching methods with simpler learning objectives and faster inference

²The recursive relationship in Eq. 2 starts from the current time step [28, 113] instead of the next time step as in some prior approaches [52, 129, 110].

speed than denoising diffusion models [63, 64, 85]. In Appendix A.2, we discuss the problem setting and the standard learning objective for flow matching.

In the context of RL, prior work has used flow matching to estimate the discounted state occupancy measure [29] by incorporating the Bellman equation (Eq. 2) into the conditional flow matching loss (Eq. 11), resulting in a temporal difference flow matching procedure (TD flows) [29]. Specifically, given a policy π , prior work models the occupancy measure p_γ^π by optimizing the vector field $v : [0, 1] \times \mathcal{S} \times \mathcal{S} \times \mathcal{A} \rightarrow \mathcal{S}$ using the following loss:

$$\begin{aligned} \mathcal{L}_{\text{TD flow}}(v) &= (1 - \gamma)\mathcal{L}_{\text{TD current flow}}(v) + \gamma\mathcal{L}_{\text{TD future flow}}(v) \\ \mathcal{L}_{\text{TD current flow}}(v) &= \mathbb{E}_{\substack{t \sim \text{UNIF}([0,1]), \epsilon \sim \mathcal{N}(0,I), \\ (s,a) \sim p^\beta(s,a)}} [\|v(t, s^t, s, a) - (s - \epsilon)\|_2^2] \\ \mathcal{L}_{\text{TD future flow}}(v) &= \mathbb{E}_{\substack{t \sim \text{UNIF}([0,1]), \epsilon \sim \mathcal{N}(0,I), \\ (s,a,s') \sim p^\beta(s,a,s'), a' \sim \pi(a'|s')}} [\|v(t, \bar{s}_f^t, s, a) - \bar{v}(t, \bar{s}_f^t, s, a)\|_2^2], \end{aligned} \quad (4)$$

where $p^\beta(s, a)$ and $p^\beta(s, a, s')$ denote the joint distribution of transitions, $s^t = ts + (1 - t)\epsilon$ is a linear interpolation between the current state s and the noise ϵ , and \bar{v} denotes an exponential moving average of historical v over iterations (a target vector field) [35, 73, 18]. Of particular note is that we obtain a target future state \bar{s}_f by applying the Euler method (Alg. 3) to \bar{v} at the next state-action pair (s', a') , where a' is sampled from the target policy π of interest, and the noisy future state $\bar{s}_f^t = t\bar{s}_f + (1 - t)\epsilon$ is a linear interpolation between this future state \bar{s}_f and the noise ϵ . Intuitively, minimizing $\mathcal{L}_{\text{TD current flow}}$ reconstructs the distribution of current state s , while minimizing $\mathcal{L}_{\text{TD future flow}}$ bootstraps the vector field v at a noisy target future state \bar{s}_f^t , similar to Q-learning [123]. Choosing the target policy π to be the same as β , we obtain a SARSA [94] variant of the loss optimizing the SARSA flows. We call the loss in Eq. 4 the TD flow loss³ and will use the SARSA variant of it to learn generative occupancy models.

4 Intention-conditioned flow occupancy models

In this section, we will introduce our method for pre-training and fine-tuning in RL. After formalizing the problem setting, we will dive into the latent variable model for pre-training an intention encoder and flow occupancy model. After pre-training the occupancy models, our method will extract policies for solving different tasks by invoking a generalized policy improvement procedure [9]. We refer to our method as **intention-conditioned flow occupancy models (InFOM)**.

4.1 Problem setting

We consider learning with purely *offline* datasets, where an unlabeled (reward-free) dataset of transitions $D = \{(s, a, s', a')\}$ collected by the behavioral policy β is provided for pre-training and a reward-labeled dataset $D_{\text{reward}} = \{(s, a, r)\}$ collected by some other policy $\tilde{\beta}$ on a downstream task is used for fine-tuning. Importantly, the behavioral policy β used to collect D can consist of a mixture of policies used by different users to complete distinct tasks. We will call this heterogeneous structure of the unlabeled datasets “intentions,” which are latent vectors z s in some latent space \mathcal{Z} . In practice, these intentions can refer to desired goal images or language instructions that index the behavioral policy $\beta = \{\beta(\cdot | \cdot, z) : z \in \mathcal{Z}\}$. Because these latent intentions are *unobserved* to the pre-training algorithm, we want to infer them as a latent random variable Z from the offline dataset, similar to prior work [40, 62, 43].

During pre-training, our method exploits the heterogeneous structure of the unlabeled dataset and extracts actionable information by (1) inferring intentions of the data collection policy and (2) learning occupancy models to predict long-horizon future states based on those intentions (Sec. 4.2 & 4.3). During fine-tuning, we first recover a set of intention-conditioned Q functions by regressing towards average rewards at future states generated by the occupancy models, and then extract a policy to maximize task-specific discounted cumulative returns (Sec. 4.4). Our method builds upon an assumption regarding the consistency of latent intentions.

Assumption 1 (Consistency). *The unlabeled dataset D for pre-training is obtained by executing a behavioral policy following a mixture of unknown intentions $z \in \mathcal{Z}$. We assume that consecutive transitions (s, a) and (s', a') share the same intention.*

³The TD flow loss is called the TD²-CFM loss in Farebrother et al. [29] and we rename it for simplicity.

The consistency of intentions across transitions enables both intention inference using two sets of transitions and dynamic programming over trajectory segments.

4.2 Variational intention inference

The goal of our pre-training framework is to learn a latent variable model that capture both long-horizon temporal information and unknown user intentions in the unlabeled datasets.

This part of our method aims to infer the intention z based on consecutive transitions (s, a, s', a') using the encoder $p_e(z | s', a')$ and predict the occupancy measures of a future state s_f using the occupancy models $q_d(s_f | s, a, z)$. We want to maximize the likelihood of observing a future state s_f starting from a state-action pair (s, a) (amortized variational inference [57, 69]), both sampled from the unlabeled dataset D following the joint behavioral distribution $p^\beta(s, a, s_f) = p^\beta(s, a)p^\beta(s_f | s, a)$:

$$\max_{q_d} \mathbb{E}_{p^\beta(s, a, s_f)} [\log q_d(s_f | s, a)] \geq \max_{p_e, q_d} L(p_e, q_d),$$

$$L(p_e, q_d) \triangleq \mathbb{E}_{p^\beta(s, a, s_f, s', a')} [\mathbb{E}_{p_e(z | s', a')} [\log q_d(s_f | s, a, z)] - \lambda D_{\text{KL}}(p_e(z | s', a') \| p(z))], \quad (5)$$

where $p(z) = \mathcal{N}(0, I)$ denotes an uninformative standard Gaussian prior over intentions and λ denotes the coefficient that controls the strength of the KL divergence regularization. We defer the full derivation of the evidence lower bound (ELBO) $L(p_e, q_d)$ to Appendix B.1. Inferring the intention z from the next transition (s', a') follows from our consistency assumption (Assump. 1), and is important for avoiding overfitting [31]. Importantly, p_e and q_d are optimized *jointly* with this objective. One way of understanding this ELBO is as maximizing an information bottleneck with the chain of random variables $(S', A') \rightarrow Z \rightarrow (S, A, S_f)$. See Appendix B.1 for the connection.

We use flow matching to reconstruct the discounted state occupancy measure rather than maximizing the likelihood directly, resulting in minimizing a surrogate objective:

$$\min_{p_e, q_d} \mathcal{L}_{\text{Flow}}(q_d, p_e) + \lambda \mathbb{E}_{p^\beta(s', a')} [D_{\text{KL}}(p_e(z | s', a') \| p(z))]. \quad (6)$$

We use $\mathcal{L}_{\text{Flow}}$ to denote a placeholder for the flow matching loss and will instantiate this loss for the flow occupancy models q_d next.

4.3 Predicting the future via SARSA flows

We now present the objective used to learn the flow occupancy models, where we first introduce some motivations and desiderata and then specify the actual loss. Given an unlabeled dataset D and an intention encoder $p_e(z | s', a')$, the goal is to learn a *generative* occupancy model $q_d(s_f | s, a, z)$ that approximates the discounted state occupancy measure of the behavioral policy conditioned on different intentions, i.e., $q_d(s_f | s, a, z) \approx p^\beta(s_f | s, a, z)$. We will use $v_d : [0, 1] \times \mathcal{S} \times \mathcal{S} \times \mathcal{A} \times \mathcal{Z} \rightarrow \mathcal{S}$ to denote the time-dependent vector field that corresponds to q_d . There are two desired properties of the learned occupancy models: (1) distributing the peak probability density to multiple s_f , i.e., modeling multimodal structure, and (2) stitching together trajectory segments that share some transitions in the dataset, i.e., enabling combinatorial generalization. The first property motivates us to use an expressive flow-matching model [64], while the second property motivates us to learn those occupancy models using temporal difference approaches [52, 112, 29]. Prior work [29] has derived the TD version of the regular (Monte Carlo) flow matching loss (Eq. 11) that incorporates the Bellman backup into the flow matching procedure, showing the superiority in sample efficiency and the capability of dynamic programming. We will adopt the same idea and use the SARSA variant of the TD flow loss (Eq. 4) to learn our intention-conditioned flow occupancy models:

$$\mathcal{L}_{\text{SARSA flow}}(v_d, p_e) = (1 - \gamma) \mathcal{L}_{\text{SARSA current flow}}(v_d, p_e) + \gamma \mathcal{L}_{\text{SARSA future flow}}(v_d, p_e), \quad (7)$$

$$\mathcal{L}_{\text{SARSA current flow}}(v_d, p_e) = \mathbb{E}_{\substack{(s, a, s', a') \sim p^\beta(s, a, s', a'), \\ z \sim p_e(z | s', a'), \\ t \sim \text{UNIF}([0, 1]), \epsilon \sim \mathcal{N}(0, I)}} [\|v(t, s^t, s, a, z) - (s - \epsilon)\|_2^2],$$

$$\mathcal{L}_{\text{SARSA future flow}}(v_d, p_e) = \mathbb{E}_{\substack{(s, a, s', a') \sim p^\beta(s, a, s', a'), \\ z \sim p_e(z | s', a'), \\ t \sim \text{UNIF}([0, 1]), \epsilon \sim \mathcal{N}(0, I)}} [\|v_d(t, \bar{s}_f^t, s, a, z) - \bar{v}_d(t, \bar{s}_f^t, s, a, z)\|_2^2].$$

Importantly, incorporating the information from latent intentions into the flow occupancy models allows us to (1) use the simpler and more stable SARSA bootstrap instead of the Q-learning style

bootstrap (Eq. 4) on large datasets, (2) generalize over latent intentions, avoiding counterfactual errors, and (3) prevent learning standalone intention-conditioned policies explicitly using offline RL algorithms (See Sec. 5.2 for further discussion and empirical studies).

4.4 Generative value estimation and implicit generalized policy improvement

We next discuss the fine-tuning process in our algorithm. Our fine-tuning method builds on the dual perspective of value estimation introduced in the preliminaries (Eq. 3). We first estimate a *set* of intention-conditioned Q functions using regression and then use those intention-conditioned Q functions to extract a policy, utilizing generalized policy improvement (GPI) [9]. The key idea of GPI is that, in addition to taking the maximum over the actions, we can also take the maximum over the intentions. In our setting, the number of intentions is infinite—one for every choice of continuous z . Thus, taking the maximum over the intentions is both nontrivial and susceptible to instability (Sec. 5.3). We address this issue by replacing the greedy “max” with an upper expectile loss, resulting in an implicit generalized policy improvement procedure.

Generative value estimation. Given a reward-labeled dataset D_{reward} and the pre-trained flow occupancy models q_d , we can estimate intention-conditioned Q values for a downstream task. Specifically, for a fixed latent intention $z \in \mathcal{Z}$, we first sample a set of N future states from the flow occupancy models, $s_f^{(1)}, \dots, s_f^{(N)} : s_f^{(i)} \sim q_d(s_f | s, a, z)$, and then constructs a Monte Carlo (MC) estimation of the Q function using those generative samples:⁴

$$\hat{Q}(s, a, z) = \frac{1}{(1-\gamma)N} \sum_{i=1}^N r(s_f^{(i)}), s_f^{(i)} \sim q_d(s_f | s, a, z),$$

where $r(\cdot)$ is the ground truth reward function or a learned reward predictor.

Implicit generalized policy improvement. We can then use those MC estimation of Q functions to learn a policy by invoking the generalized policy improvement. The naïve GPI requires sampling a finite set of latent intentions from the prior distribution $p(z)$,⁵ $z^{(1)}, \dots, z^{(M)} : z^{(j)} \sim p(z)$ and greedily choose one \hat{Q} to update the policy:

$$\arg \max_{\pi} \mathbb{E}_{\substack{s \sim p^{\tilde{\beta}}(s), a \sim \pi(a|s) \\ z^{(1)}, \dots, z^{(M)} : z^{(j)} \sim p(z)}} \left[\max_{z^{(j)}} \hat{Q}(s, a, z) \right].$$

Despite its simplicity, the naïve GPI suffers from two main disadvantages. First, using the maximum Q over a finite set of latent intentions to approximate the maximum Q over an infinite number of intentions results in local optima. Second, when we take gradients of this objective with respect to the policy, the chain rule gives one term involving $\nabla_a q_d(s_f | s, a, z)$. Thus, computing the gradients requires differentiating through the ODE solver (backpropagating through time [85]), which is unstable. We address these challenges by learning an explicit scalar Q function to distill the MC estimation of intention-conditioned Q functions. This approach is appealing because gradients of the Q function no longer backpropagate through the ODE solver. We also replace the “max” over a finite set of intention-conditioned Q functions with an upper expectile loss L_2^μ [58], resulting in the following critic loss

$$\mathcal{L}(Q) = \mathbb{E}_{(s,a) \sim p^{\tilde{\beta}}(s,a), z \sim p(z)} \left[L_2^\mu \left(Q(s, a) - \hat{Q}(s, a, z) \right) \right], \quad (8)$$

where $L_2^\mu(x) = |\mu - \mathbb{1}(x < 0)|x^2$ and $\mu \in [0.5, 1)$. After distilling the intention-conditioned Q functions into a single function, we can extract the policy by selecting actions to maximize Q with a behavioral cloning regularization [32] using the actor loss

$$\mathcal{L}(\pi) = -\mathbb{E}_{(s,a) \sim p^{\tilde{\beta}}(s,a), a^\pi \sim \pi(a^\pi|s)} [Q(s, a^\pi) + \alpha \log \pi(a | s)], \quad (9)$$

where α controls the regularization strength. Taken together, we call the expectile Q distillation step (Eq. 8) and the policy optimization step (Eq. 9) *implicit generalized policy improvement (implicit GPI)*. In Appendix B.2, we discuss the intuition and theoretical soundness of the implicit GPI.

⁴We omit the dependency of \hat{Q} on $s_f^{(1)}, \dots, s_f^{(N)}$ to simplify notations.

⁵We choose to sample from the prior $p(z)$ because of the KL divergence in $L(p_e, q_d)$, resembling the generation of random samples from a variational auto-encoder [57].

Algorithm 1 Intention-Conditioned Flow Occupancy Model (pre-training).

- 1: **Input** The intention encoder p_ϕ , the vector field v_θ , the target vector field $v_{\bar{\theta}}$, the policy π_ω , and the reward-free dataset D .
 - 2: **for** each iteration **do**
 - 3: Sample a batch of $\{(s, a, s', a') \sim D\}$.
 - 4: Sample a batch of $\{\epsilon \sim \mathcal{N}(0, I)\}$ and a batch of $\{t \sim \text{UNIF}([0, 1])\}$.
 - 5: Encode intentions $\{z \sim p_\phi(z \mid s', a')\}$ for each (s', a') .
 ∇ **SARSA flow occupancy model loss.**
 - 6: $s^t \leftarrow (1 - t)\epsilon + ts$
 - 7: $\bar{s}_f \leftarrow \text{EulerMethod}(v_{\bar{\theta}}, \epsilon, s', a', z), \bar{s}_f^t \leftarrow (1 - t)z + t\bar{s}_f$.
 - 8: $\mathcal{L}_{\text{SARSA current flow}}(\theta, \phi) \leftarrow \mathbb{E}_{(s, a, z, t, \epsilon, s^t)} [\|v_\theta(t, s^t, s, a, z) - (s - z)\|_2^2]$.
 - 9: $\mathcal{L}_{\text{SARSA future flow}}(\theta, \phi) \leftarrow \mathbb{E}_{(s, a, z, t, \epsilon, \bar{s}_f^t)} [\|v_\theta(t, \bar{s}_f^t, s, a, z) - v_{\bar{\theta}}(t, \bar{s}_f^t, s, a, z)\|_2^2]$.
 - 10: $\mathcal{L}_{\text{SARSA flow}}(\theta, \phi) \leftarrow (1 - \gamma)\mathcal{L}_{\text{current}}(\theta, \phi) + \gamma\mathcal{L}_{\text{future}}(\theta, \phi)$.
 ∇ **Intention encoder loss.**
 - 11: $\mathcal{L}_{\text{ELBO}}(\theta, \phi) \leftarrow \mathcal{L}_{\text{SARSA flow}}(\theta, \phi) + \lambda \mathbb{E}_{(s', a')} [D_{\text{KL}}(p_\phi(z \mid s', a') \parallel \mathcal{N}(0, I))]$.
 ∇ **(Optional) Behavioral cloning loss.**
 - 12: $\mathcal{L}_{\text{BC}}(\omega) \leftarrow -\mathbb{E}_{(s, a)} [\log \pi_\omega(a \mid s)]$.
 - 13: Update the vector field θ and the intention encoder ϕ by minimizing $\mathcal{L}_{\text{ELBO}}(\theta, \phi)$.
 - 14: Update the policy ω by minimizing $\mathcal{L}_{\text{BC}}(\omega)$.
 - 15: Update the target vector field $\bar{\theta}$ using an exponential moving average of θ .
 - 16: **Return** v_θ, p_ϕ , and π_ω .
-

Algorithm summary. We use neural networks to parameterize the intention encoder p_ϕ , the vector field of the occupancy models v_θ , the reward predictor r_η , the critic Q_ψ , and the policy π_ω . We consider two stages: pre-training and fine-tuning. In Alg. 1, we summarize the pre-training process of InFOM. InFOM pre-trains (1) the vector field v_θ using the SARSA flow loss (Eq. 7) and (2) the intention encoder p_ϕ using the ELBO (Eq. 5). Alg. 2 shows the pseudocode of InFOM for fine-tuning. InFOM mainly learns (1) the reward predictor r_η via simple regression, (2) the critic Q_ψ using expectile distillation (Eq. 8), and (3) the policy π_ω by conservatively maximizing the Q (Eq. 9). The open-source implementation is available online.⁶

5 Experiments

Our experiments start with comparing InFOM to prior methods that first pre-train on reward-free datasets and then fine-tune on reward-labeled datasets, measuring the performance on downstream tasks. The models pre-trained by those methods include behavioral cloning policies, transition models, representations, discriminative classifiers that predict occupancy measures, and latent intentions along with intention-conditioned policies (skills). We then conduct ablations studying the two main components of our method: the variational intention encoder and the implicit GPI policy extraction strategy. Analyzing the convergence speed reveals that our flow occupancy models enable faster policy learning. All experiments report means and standard deviations across 8 random seeds for state-based tasks and 4 random seeds for image-based tasks.

5.1 Comparing to prior pre-training and fine-tuning methods

Our experiments study whether the proposed method (InFOM), which captures actionable information conditioned on user intentions from unlabeled datasets, can train efficient policies to solve downstream tasks after fine-tuning. On 36 state-based and 4 image-based tasks across diverse robotic navigation and manipulation domains (Appendix C.1), we compare the performance of InFOM against eight baselines (Appendix C.2) after first pre-training and then fine-tuning each method for a fixed number of gradient steps. Following prior practice [85, 106], we report returns or success rates at the end

⁶<https://github.com/chongyi-zheng/infom>

Algorithm 2 Intention-Conditioned Flow Occupancy Model (fine-tuning).

- 1: **Input** The intention encoder p_ϕ , the vector field v_θ , the target vector field $v_{\bar{\theta}}$, the reward predictor r_η , the critic Q_ψ , the policy π_ω , and the reward-labeled dataset D_{reward} .
 - 2: **for** each iteration **do**
 - 3: Sample a batch of $\{(s, a, r, s', a') \sim D_{\text{reward}}\}$.
 - 4: Sample a batch of $\{\epsilon \sim \mathcal{N}(0, I)\}$ and a batch of $\{t \sim \text{UNIF}([0, 1])\}$.
 - 5: Sample prior intentions $\{z \sim p(z)\}$.
 - 6: Sample a batch of $\{(\epsilon^{(1)}, \dots, \epsilon^{(N)}) \sim (\mathcal{N}(0, I), \dots, \mathcal{N}(0, I))\}$.
 ∇ **SARSA flow occupancy model loss and intention encoder loss.**
 - 7: $\mathcal{L}_{\text{ELBO}}(\theta, \psi)$ as in Alg. 1.
 ∇ **Reward predictor loss.**
 - 8: $\mathcal{L}_{\text{Reward}}(\eta) \leftarrow \mathbb{E}_{(s, r)} [(r_\eta(s) - r)^2]$.
 ∇ **Critic loss.**
 - 9: $s_f^{(i)} \leftarrow \text{EulerMethod}(v_\theta, \epsilon^{(i)}, s, a, z)$ (Alg. 3) for each $(s, a, z, \epsilon^{(i)})$.
 - 10: $\hat{Q}(s, a, z) \leftarrow \frac{1}{(1-\gamma)N} \sum_{i=1}^N r_\eta(s_f^{(i)})$.
 - 11: $\mathcal{L}_{\text{Critic}}(\psi) \leftarrow \mathbb{E}_{(s, a, z, s_f^{(1)}, \dots, s_f^{(N)})} \left[L_2^\mu \left(Q_\psi(s, a) - \hat{Q}(s, a, z) \right) \right]$.
 ∇ **Actor loss.**
 - 12: $\mathcal{L}_{\text{Actor}}(\omega) \leftarrow -\mathbb{E}_{(s, a), a^\pi \sim \pi_\omega(a^\pi | s)} [Q_\psi(s, a^\pi) + \alpha \log \pi_\omega(a | s)]$.
 - 13: Update the vector field θ and the intention encoder ϕ by minimizing $\mathcal{L}_{\text{ELBO}}(\theta, \phi)$.
 - 14: Update the reward predictor η , the critic ψ , and the policy ω by minimizing $\mathcal{L}_{\text{Reward}}(\eta)$, $\mathcal{L}_{\text{Critic}}(\psi)$, and $\mathcal{L}_{\text{Actor}}(\omega)$ respectively.
 - 15: Update the target vector field $\bar{\theta}$ using an exponential moving average of θ .
 - 16: **Return** $v_\theta, p_\phi, r_\eta, Q_\psi$, and π_ω .
-



Figure 2: **Domains for evaluation.** (Left) ExORL domains (16 state-based tasks). (Right) OGBench domains (20 state-based tasks and 4 image-based tasks).

of fine-tuning instead of the best performance across all evaluation steps to prevent bias. Whenever possible, we use the same hyperparameters for all methods. See Appendix C.3 for details of the evaluation protocol and Appendix C.4 for implementations and hyperparameters of each method.

We report results in Fig. 3, aggregating over four tasks in each domain of ExORL and five tasks in each domain of OGBench, and present the full results in Table 4. These results show that InFOM matches or surpasses all baselines on six out of eight domains. On ExORL benchmarks, all methods perform similarly on the two easier domains (cheetah and quadruped), while InFOM is able to obtain $20\times$ improvement on jaco, where baselines only make trivial progress (Table 4). On those more challenging state-based manipulation tasks from OGBench, we find a marked difference between baselines and InFOM; our method achieves 36% higher success rate over the best performing baseline. In addition, InFOM is able to outperform the best baseline by 31% using RGB images as input directly (visual tasks). We hypothesize that the baselines fail to solve these more challenging tasks because of the semi-sparse reward functions, while our method learns an expressive generative model along with the GPI-like policy extraction strategy to better exploit the high-reward region of the state space.

5.2 Variational intention inference is simple and performant

We now conduct experiments ablating a key component in our method: the variational intention encoder. To investigate whether this framework induces a simple and performant way to infer diverse

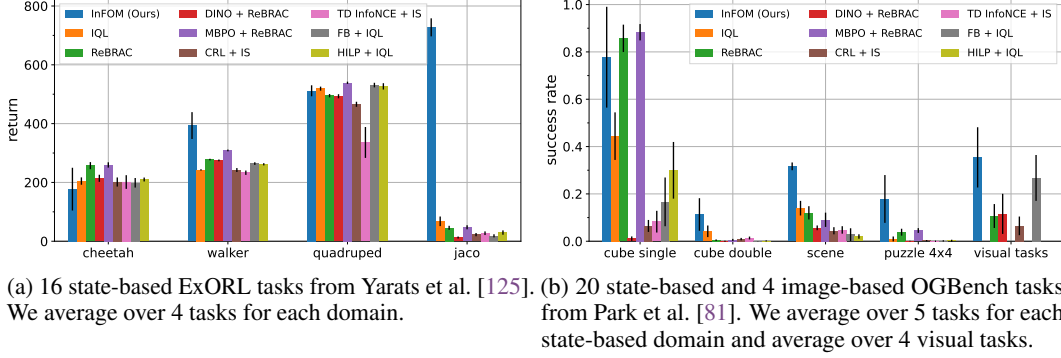


Figure 3: **Evaluation on ExORL and OGBench tasks.** We compare InFOM against prior methods that utilize various learning paradigms on task-agnostic pre-training and task-specific fine-tuning. InFOM performs similarly to, if not better than, prior methods on 7 out of the 9 domains, including the most challenging visual tasks. We report means and standard deviations over 8 random seeds (4 random seeds for image-based tasks) with error bars indicating one standard deviation. See Table 4 for full results.

user intentions from an unlabeled dataset, we compare it to various intention encoding mechanisms proposed by prior methods. Specifically, we consider replacing the variational intention encoder with either (1) a set of Hilbert representations and Hilbert foundation policies [84] (HILP + FOM) or (2) a set of forward-backward representations and representation-conditioned policies [113] (FB + FOM), and then pre-training the flow occupancy models conditioned on these two sets of representations. Note that FB + FOM is equivalent to TD flows with GPI in Farebrother et al. [29]. We choose two tasks in the ExORL benchmarks (walker flip and quadruped jump) and another two tasks taken from the OGBench benchmarks (cube double task 1 and scene task 1), following the same evaluation protocols as in Appendix C.3.

Results in Fig. 4 indicate that InFOM can outperform prior intention encoding methods on 3 out of 4 tasks, while being simpler. Both HILP and FB capture intentions with full unsupervised RL objectives based on an actor-critic backbone. In contrast, we capture intentions by simply training an intention encoder based on a latent variable model over adjacent transitions, without relying on a potentially complicated offline RL procedure [106, 82].

5.3 Importance of the implicit generalized policy improvement

The next experiments study different approaches for policy optimization. We hypothesize that our proposed method is more efficient and robust than other policy extraction strategies. To test this hypothesis, we conduct ablation experiments on one task in the ExORL benchmarks (quadruped jump) and another task taken from the OGBench benchmarks (scene task 1), again following the evaluation protocols in Appendix C.3. We compare two alternative policy learning approaches in the fine-tuning phase. First, we ablate the effect of the upper expectile loss by comparing against the standard GPI, which maximizes Q functions over a finite set of intentions $\{z^{(1)}, \dots, z^{(M)}\}$. We choose $M = 32$ latent intentions to balance between performance and compute budget, and call this variant InFOM + GPI. Second, we ablate the effect of the variational intention encoder by removing the intention dependency in the flow occupancy models and extracting the policy via one-step policy improvement (PI) [121, 14, 89, 88]. We call this method FOM + one-step PI and defer the detailed formulation into Appendix B.3.

As shown in Fig. 5, InFOM achieves significantly higher returns and success rates than its variant based on one-step policy improvement, suggesting the importance of inferring user intentions. Compared with its GPI counterpart, our method is 44% more performant with $8\times$ smaller variance (the error bar indicates one standard deviation), demonstrating that the implicit GPI indeed performs a relaxed maximization over intentions while maintaining robustness.

5.4 Flow occupancy models enable faster policy learning

We then investigate whether the proposed method leads to faster policy learning on downstream tasks. We answer this question by an ablation study with a high evaluation frequency, analyzing the performance of various methods throughout the entire fine-tuning phase every 2K gradient steps.

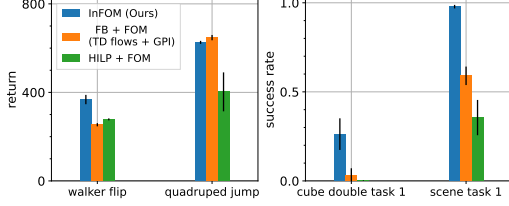


Figure 4: Comparison to prior intention encoding mechanisms. We compare InFOM to prior intention encoding mechanisms based on unsupervised skill discovery (HILP [84]) or successor feature learning (FB [113]). FB + FOM is equivalent to TD flows with GPI in Farebrother et al. [29]. We observe that InFOM outperforms prior methods on 3 out of the 4 tasks. See Sec. 5.2 for details.

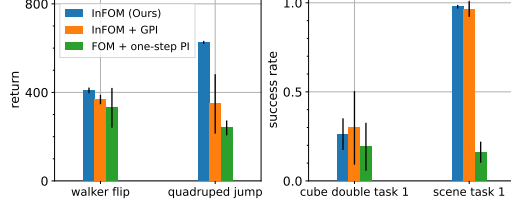


Figure 5: Comparison to alternative policy extraction strategies. We compare InFOM to alternative policy extraction strategies based on the standard generalized policy improvement or one-step policy improvement. Our method is 44% more performant with $8\times$ smaller variance than the variant using the standard GPI. See Sec. 5.3 for details.

We compare InFOM to prior methods on two ExORL tasks (cheetah run and quadruped jump), including ReBRAC, CRL + IS, DINO + ReBRAC, MBPO + ReBRAC, and FB + IQL (See Sec. 5.1 for details of these baselines). We choose these baselines because they perform similarly to our method, helping to prevent counterfactual errors derived from the performance deviation when comparing convergence speed.

We compare different algorithms by plotting the returns at each evaluation step, with the shaded regions indicating one standard deviation. As shown in Fig. 6, InFOM converges faster than prior methods that only pre-train behavioral cloning policies (ReBRAC) or self-supervised state representations (DINO + ReBRAC), demonstrating the effectiveness of extracting temporal information. The observation that methods utilizing a one-step transition model (MBPO + ReBRAC) or a future state classifier (CRL + IS) learn slower than our method highlights the importance of predicting long-horizon future events using expressive generative models. Additionally, our flow occupancy models extract rich latent intentions from the unlabeled datasets, resulting in adaptation speed similar to the prior zero-shot RL method (FB + IQL).

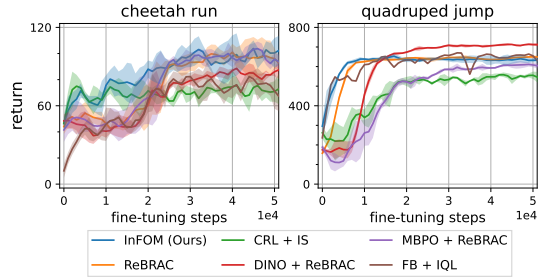


Figure 6: Convergence speed during fine-tuning. On tasks where InFOM and baselines perform similarly, our flow occupancy models enable faster policy learning.

6 Conclusion

In this work, we presented InFOM, a method that captures diverse intentions and their long-term behaviors from an unstructured dataset, leveraging the expressivity of flow models. We empirically showed that the intentions captured in flow occupancy models enable effective and efficient fine-tuning, outperforming prior unsupervised pre-training approaches on diverse state- and image-based domains.

Limitations. One limitation of InFOM is that our reduction from trajectories to consecutive state-action pairs might not always accurately capture the original intentions in the trajectories. While we empirically showed that this simple approach is sufficient to achieve strong performance on our benchmark tasks, it can be further improved with alternative trajectory encoding techniques and data collection strategies, which we leave for future work.

Acknowledgments and disclosure of funding

We thank Kevin Frans, Homer Walker, Aravind Venugopal, and Bogdan Mazouze for their helpful discussions. We also thank Tongzhou Wang for sharing code during the early stages of our experiments. This work used the Della computational cluster provided by Princeton Research Computing, as well as the Ionic and Neuronic computing clusters maintained by the Department of Computer Science at Princeton University. This research was partly supported by the Korea Foundation for Advanced Studies (KFAS) and ONR N00014-22-1-2773.

References

- [1] Achiam, J., Adler, S., Agarwal, S., Ahmad, L., Akkaya, I., Aleman, F. L., Almeida, D., Al-tenschmidt, J., Altman, S., Anadkat, S., et al. (2023). Gpt-4 technical report. *arXiv preprint arXiv:2303.08774*.
- [2] Ajay, A., Du, Y., Gupta, A., Tenenbaum, J. B., Jaakkola, T. S., and Agrawal, P. (2023). Is conditional generative modeling all you need for decision making? In *The Eleventh International Conference on Learning Representations*.
- [3] Ajay, A., Kumar, A., Agrawal, P., Levine, S., and Nachum, O. (2021). OPAL: Offline primitive discovery for accelerating offline reinforcement learning. In *International Conference on Learning Representations*.
- [4] Albergo, M. S. and Vanden-Eijnden, E. (2023). Building normalizing flows with stochastic interpolants. In *The Eleventh International Conference on Learning Representations*.
- [5] Alemi, A. A., Fischer, I., Dillon, J. V., and Murphy, K. (2017). Deep variational information bottleneck. In *International Conference on Learning Representations*.
- [6] Alonso, E., Jelley, A., Micheli, V., Kanervisto, A., Storkey, A. J., Pearce, T., and Fleuret, F. (2024). Diffusion for world modeling: Visual details matter in atari. *Advances in Neural Information Processing Systems*, 37:58757–58791.
- [7] Barber, D. and Agakov, F. (2004). The im algorithm: a variational approach to information maximization. *Advances in neural information processing systems*, 16(320):201.
- [8] Barreto, A., Borsa, D., Quan, J., Schaul, T., Silver, D., Hessel, M., Mankowitz, D., Zidek, A., and Munos, R. (2018). Transfer in deep reinforcement learning using successor features and generalised policy improvement. In *International Conference on Machine Learning*, pages 501–510. PMLR.
- [9] Barreto, A., Dabney, W., Munos, R., Hunt, J. J., Schaul, T., van Hasselt, H. P., and Silver, D. (2017). Successor features for transfer in reinforcement learning. *Advances in neural information processing systems*, 30.
- [10] Black, K., Brown, N., Driess, D., Esmail, A., Equi, M., Finn, C., Fusai, N., Groom, L., Hausman, K., Ichter, B., et al. (2024). π_0 : A vision-language-action flow model for general robot control. *arXiv preprint arXiv:2410.24164*.
- [11] Blier, L., Tallec, C., and Ollivier, Y. (2021). Learning successor states and goal-dependent values: A mathematical viewpoint. *arXiv preprint arXiv:2101.07123*.
- [12] Borsa, D., Barreto, A., Quan, J., Mankowitz, D., Munos, R., Van Hasselt, H., Silver, D., and Schaul, T. (2018). Universal successor features approximators. *arXiv preprint arXiv:1812.07626*.
- [13] Bradbury, J., Frostig, R., Hawkins, P., Johnson, M. J., Leary, C., Maclaurin, D., Necula, G., Paszke, A., VanderPlas, J., Wanderman-Milne, S., and Zhang, Q. (2018). JAX: composable transformations of Python+NumPy programs.
- [14] Brandfonbrener, D., Whitney, W., Ranganath, R., and Bruna, J. (2021). Offline rl without off-policy evaluation. *Advances in neural information processing systems*, 34:4933–4946.

- [15] Brown, T., Mann, B., Ryder, N., Subbiah, M., Kaplan, J. D., Dhariwal, P., Neelakantan, A., Shyam, P., Sastry, G., Askell, A., et al. (2020). Language models are few-shot learners. *Advances in neural information processing systems*, 33:1877–1901.
- [16] Burda, Y., Edwards, H., Storkey, A., and Klimov, O. (2019). Exploration by random network distillation. In *International Conference on Learning Representations*.
- [17] Campbell, A., Yim, J., Barzilay, R., Rainforth, T., and Jaakkola, T. (2024). Generative flows on discrete state-spaces: Enabling multimodal flows with applications to protein co-design. In *International Conference on Machine Learning*, pages 5453–5512. PMLR.
- [18] Caron, M., Touvron, H., Misra, I., Jégou, H., Mairal, J., Bojanowski, P., and Joulin, A. (2021). Emerging properties in self-supervised vision transformers. In *Proceedings of the IEEE/CVF international conference on computer vision*, pages 9650–9660.
- [19] Chen, B., Zhu, C., Agrawal, P., Zhang, K., and Gupta, A. (2023). Self-supervised reinforcement learning that transfers using random features. *Advances in Neural Information Processing Systems*, 36:56411–56436.
- [20] Chen, L., Lu, K., Rajeswaran, A., Lee, K., Grover, A., Laskin, M., Abbeel, P., Srinivas, A., and Mordatch, I. (2021). Decision transformer: Reinforcement learning via sequence modeling. *Advances in neural information processing systems*, 34:15084–15097.
- [21] Dayan, P. (1993). Improving generalization for temporal difference learning: The successor representation. *Neural computation*, 5(4):613–624.
- [22] Devlin, J., Chang, M.-W., Lee, K., and Toutanova, K. (2019). Bert: Pre-training of deep bidirectional transformers for language understanding. In *Proceedings of the 2019 conference of the North American chapter of the association for computational linguistics: human language technologies, volume 1 (long and short papers)*, pages 4171–4186.
- [23] Ding, Z., Zhang, A., Tian, Y., and Zheng, Q. (2024). Diffusion world model. *arXiv e-prints*, pages arXiv–2402.
- [24] Durrett, R. (2019). *Probability: theory and examples*, volume 49. Cambridge university press.
- [25] Espeholt, L., Soyer, H., Munos, R., Simonyan, K., Mnih, V., Ward, T., Doron, Y., Firoiu, V., Harley, T., Dunning, I., et al. (2018). Impala: Scalable distributed deep-rl with importance weighted actor-learner architectures. In *International conference on machine learning*, pages 1407–1416. PMLR.
- [26] Eysenbach, B., Gupta, A., Ibarz, J., and Levine, S. (2019). Diversity is all you need: Learning skills without a reward function. In *International Conference on Learning Representations*.
- [27] Eysenbach, B., Salakhutdinov, R., and Levine, S. (2020). C-learning: Learning to achieve goals via recursive classification. *arXiv preprint arXiv:2011.08909*.
- [28] Eysenbach, B., Zhang, T., Levine, S., and Salakhutdinov, R. R. (2022). Contrastive learning as goal-conditioned reinforcement learning. *Advances in Neural Information Processing Systems*, 35:35603–35620.
- [29] Farebrother, J., Pirotta, M., Tirinzoni, A., Munos, R., Lazaric, A., and Touati, A. (2025). Temporal difference flows. In *ICLR 2025 Workshop on World Models: Understanding, Modelling and Scaling*.
- [30] Frans, K., Hafner, D., Levine, S., and Abbeel, P. (2025). One step diffusion via shortcut models. In *The Thirteenth International Conference on Learning Representations*.
- [31] Frans, K., Park, S., Abbeel, P., and Levine, S. (2024). Unsupervised zero-shot reinforcement learning via functional reward encodings. In *International Conference on Machine Learning*, pages 13927–13942. PMLR.
- [32] Fujimoto, S. and Gu, S. S. (2021). A minimalist approach to offline reinforcement learning. *Advances in neural information processing systems*, 34:20132–20145.

- [33] Fujimoto, S., Hoof, H., and Meger, D. (2018). Addressing function approximation error in actor-critic methods. In *International conference on machine learning*, pages 1587–1596. PMLR.
- [34] Ghosh, D., Bhateja, C. A., and Levine, S. (2023). Reinforcement learning from passive data via latent intentions. In *International Conference on Machine Learning*, pages 11321–11339. PMLR.
- [35] Grill, J.-B., Strub, F., Altché, F., Tallec, C., Richemond, P., Buchatskaya, E., Doersch, C., Avila Pires, B., Guo, Z., Gheshlaghi Azar, M., et al. (2020). Bootstrap your own latent-a new approach to self-supervised learning. *Advances in neural information processing systems*, 33:21271–21284.
- [36] Haarnoja, T., Zhou, A., Abbeel, P., and Levine, S. (2018). Soft actor-critic: Off-policy maximum entropy deep reinforcement learning with a stochastic actor. In *International conference on machine learning*, pages 1861–1870. Pmlr.
- [37] Hafner, D., Pasukonis, J., Ba, J., and Lillicrap, T. (2023). Mastering diverse domains through world models. *arXiv preprint arXiv:2301.04104*.
- [38] Hansen, S., Dabney, W., Barreto, A., Van de Wiele, T., Warde-Farley, D., and Mnih, V. (2019). Fast task inference with variational intrinsic successor features. *arXiv preprint arXiv:1906.05030*.
- [39] Hansen-Estruch, P., Kostrikov, I., Janner, M., Kuba, J. G., and Levine, S. (2023). Idql: Implicit q-learning as an actor-critic method with diffusion policies. *arXiv preprint arXiv:2304.10573*.
- [40] Hausman, K., Chebotar, Y., Schaal, S., Sukhatme, G., and Lim, J. J. (2017). Multi-modal imitation learning from unstructured demonstrations using generative adversarial nets. *Advances in neural information processing systems*, 30.
- [41] He, K., Chen, X., Xie, S., Li, Y., Dollár, P., and Girshick, R. (2022). Masked autoencoders are scalable vision learners. In *Proceedings of the IEEE/CVF conference on computer vision and pattern recognition*, pages 16000–16009.
- [42] He, K., Fan, H., Wu, Y., Xie, S., and Girshick, R. (2020). Momentum contrast for unsupervised visual representation learning. In *Proceedings of the IEEE/CVF conference on computer vision and pattern recognition*, pages 9729–9738.
- [43] Henderson, P., Chang, W.-D., Bacon, P.-L., Meger, D., Pineau, J., and Precup, D. (2017). Optiongan: Learning joint reward-policy options using generative adversarial inverse reinforcement learning. *ArXiv*, abs/1709.06683.
- [44] Hendrycks, D. and Gimpel, K. (2016). Gaussian error linear units (gelus). *arXiv preprint arXiv:1606.08415*.
- [45] Higgins, I., Matthey, L., Pal, A., Burgess, C., Glorot, X., Botvinick, M., Mohamed, S., and Lerchner, A. (2017). beta-VAE: Learning basic visual concepts with a constrained variational framework. In *International Conference on Learning Representations*.
- [46] Ho, J., Jain, A., and Abbeel, P. (2020). Denoising diffusion probabilistic models. *Advances in neural information processing systems*, 33:6840–6851.
- [47] Hu, H., Yang, Y., Ye, J., Mai, Z., and Zhang, C. (2023). Unsupervised behavior extraction via random intent priors. *Advances in Neural Information Processing Systems*, 36:51491–51514.
- [48] Jain, A. K., Lehnert, L., Rish, I., and Berseth, G. (2023). Maximum state entropy exploration using predecessor and successor representations. *Advances in Neural Information Processing Systems*, 36:49991–50019.
- [49] Janner, M., Du, Y., Tenenbaum, J., and Levine, S. (2022). Planning with diffusion for flexible behavior synthesis. In *International Conference on Machine Learning*, pages 9902–9915. PMLR.
- [50] Janner, M., Fu, J., Zhang, M., and Levine, S. (2019). When to trust your model: Model-based policy optimization. *Advances in neural information processing systems*, 32.
- [51] Janner, M., Li, Q., and Levine, S. (2021). Offline reinforcement learning as one big sequence modeling problem. *Advances in neural information processing systems*, 34:1273–1286.

- [52] Janner, M., Mordatch, I., and Levine, S. (2020). Gamma-models: Generative temporal difference learning for infinite-horizon prediction. *Advances in neural information processing systems*, 33:1724–1735.
- [53] Jeon, S., Bewley, T., and Cullen, J. (2024). Zero-shot reinforcement learning from low quality data. *Advances in Neural Information Processing Systems*, 37:16894–16942.
- [54] Kim, J., Park, S., and Kim, G. (2022). Constrained gpi for zero-shot transfer in reinforcement learning. *Advances in Neural Information Processing Systems*, 35:4585–4597.
- [55] Kim, J., Park, S., and Levine, S. (2024). Unsupervised-to-online reinforcement learning. *arXiv preprint arXiv:2408.14785*.
- [56] Kingma, D. P. (2014). Adam: A method for stochastic optimization. *arXiv preprint arXiv:1412.6980*.
- [57] Kingma, D. P. and Welling, M. (2013). Auto-encoding variational bayes. *arXiv preprint arXiv:1312.6114*.
- [58] Kostrikov, I., Nair, A., and Levine, S. (2022). Offline reinforcement learning with implicit q-learning. In *International Conference on Learning Representations*.
- [59] Kumar, A., Zhou, A., Tucker, G., and Levine, S. (2020). Conservative q-learning for offline reinforcement learning. *Advances in neural information processing systems*, 33:1179–1191.
- [60] Lambert, N., Pister, K., and Calandra, R. (2022). Investigating compounding prediction errors in learned dynamics models. *arXiv preprint arXiv:2203.09637*.
- [61] Laskin, M., Srinivas, A., and Abbeel, P. (2020). Curl: Contrastive unsupervised representations for reinforcement learning. In *International conference on machine learning*, pages 5639–5650. PMLR.
- [62] Li, Y., Song, J., and Ermon, S. (2017). Infogail: Interpretable imitation learning from visual demonstrations. *Advances in neural information processing systems*, 30.
- [63] Lipman, Y., Chen, R. T. Q., Ben-Hamu, H., Nickel, M., and Le, M. (2023). Flow matching for generative modeling. In *The Eleventh International Conference on Learning Representations*.
- [64] Lipman, Y., Havasi, M., Holderrieth, P., Shaul, N., Le, M., Karrer, B., Chen, R. T., Lopez-Paz, D., Ben-Hamu, H., and Gat, I. (2024). Flow matching guide and code. *arXiv preprint arXiv:2412.06264*.
- [65] Liu, X., Gong, C., and qiang liu (2023). Flow straight and fast: Learning to generate and transfer data with rectified flow. In *The Eleventh International Conference on Learning Representations*.
- [66] Lu, J., Batra, D., Parikh, D., and Lee, S. (2019). Vilbert: Pretraining task-agnostic visiolinguistic representations for vision-and-language tasks. *Advances in neural information processing systems*, 32.
- [67] Ma, Y. J., Sodhani, S., Jayaraman, D., Bastani, O., Kumar, V., and Zhang, A. (2023). VIP: Towards universal visual reward and representation via value-implicit pre-training. In *The Eleventh International Conference on Learning Representations*.
- [68] Machado, M. C., Rosenbaum, C., Guo, X., Liu, M., Tesauro, G., and Campbell, M. (2017). Eigenoption discovery through the deep successor representation. *arXiv preprint arXiv:1710.11089*.
- [69] Margossian, C. C. and Blei, D. M. (2024). Amortized variational inference: When and why? In *Uncertainty in Artificial Intelligence*, pages 2434–2449. PMLR.
- [70] Mazouze, B., Eysenbach, B., Nachum, O., and Thompson, J. (2023). Contrastive value learning: Implicit models for simple offline RL. In *7th Annual Conference on Robot Learning*.
- [71] Mazzaglia, P., Verbelen, T., Dhoedt, B., Lacoste, A., and Rajeswar, S. (2022). Choreographer: Learning and adapting skills in imagination. *arXiv preprint arXiv:2211.13350*.

- [72] Mendonca, R., Rybkin, O., Daniilidis, K., Hafner, D., and Pathak, D. (2021). Discovering and achieving goals via world models. *Advances in Neural Information Processing Systems*, 34:24379–24391.
- [73] Mnih, V., Kavukcuoglu, K., Silver, D., Rusu, A. A., Veness, J., Bellemare, M. G., Graves, A., Riedmiller, M., Fidjeland, A. K., Ostrovski, G., et al. (2015). Human-level control through deep reinforcement learning. *nature*, 518(7540):529–533.
- [74] Myers, V., Zheng, C., Dragan, A., Levine, S., and Eysenbach, B. (2024). Learning temporal distances: Contrastive successor features can provide a metric structure for decision-making. In *International Conference on Machine Learning*, pages 37076–37096. PMLR.
- [75] Nair, S., Rajeswaran, A., Kumar, V., Finn, C., and Gupta, A. (2023). R3m: A universal visual representation for robot manipulation. In *Conference on Robot Learning*, pages 892–909. PMLR.
- [76] Nemecek, M. and Parr, R. (2021). Policy caches with successor features. In *International Conference on Machine Learning*, pages 8025–8033. PMLR.
- [77] Ni, T., Eysenbach, B., Seyedsalehi, E., Ma, M., Gehring, C., Mahajan, A., and Bacon, P.-L. (2024). Bridging state and history representations: Understanding self-predictive rl. *arXiv preprint arXiv:2401.08898*.
- [78] Ouyang, L., Wu, J., Jiang, X., Almeida, D., Wainwright, C., Mishkin, P., Zhang, C., Agarwal, S., Slama, K., Ray, A., et al. (2022). Training language models to follow instructions with human feedback. *Advances in neural information processing systems*, 35:27730–27744.
- [79] O’Neill, A., Rehman, A., Maddukuri, A., Gupta, A., Padalkar, A., Lee, A., Pooley, A., Gupta, A., Mandlekar, A., Jain, A., et al. (2024). Open x-embodiment: Robotic learning datasets and rt-x models: Open x-embodiment collaboration 0. In *2024 IEEE International Conference on Robotics and Automation (ICRA)*, pages 6892–6903. IEEE.
- [80] Parisi, S., Rajeswaran, A., Purushwalkam, S., and Gupta, A. (2022). The unsurprising effectiveness of pre-trained vision models for control. In *international conference on machine learning*, pages 17359–17371. PMLR.
- [81] Park, S., Frans, K., Eysenbach, B., and Levine, S. (2025a). OGBench: Benchmarking offline goal-conditioned RL. In *The Thirteenth International Conference on Learning Representations*.
- [82] Park, S., Frans, K., Levine, S., and Kumar, A. (2024a). Is value learning really the main bottleneck in offline rl? *arXiv preprint arXiv:2406.09329*.
- [83] Park, S., Ghosh, D., Eysenbach, B., and Levine, S. (2023a). Hiql: Offline goal-conditioned rl with latent states as actions. *Advances in Neural Information Processing Systems*, 36:34866–34891.
- [84] Park, S., Kreiman, T., and Levine, S. (2024b). Foundation policies with hilbert representations. In *International Conference on Machine Learning*, pages 39737–39761. PMLR.
- [85] Park, S., Li, Q., and Levine, S. (2025b). Flow q-learning. *arXiv preprint arXiv:2502.02538*.
- [86] Park, S., Rybkin, O., and Levine, S. (2023b). Metra: Scalable unsupervised rl with metric-aware abstraction. *arXiv preprint arXiv:2310.08887*.
- [87] Pertsch, K., Lee, Y., and Lim, J. (2021). Accelerating reinforcement learning with learned skill priors. In *Conference on robot learning*, pages 188–204. PMLR.
- [88] Peters, J., Mulling, K., and Altun, Y. (2010). Relative entropy policy search. In *Proceedings of the AAAI Conference on Artificial Intelligence*, volume 24, pages 1607–1612.
- [89] Peters, J. and Schaal, S. (2007). Reinforcement learning by reward-weighted regression for operational space control. In *Proceedings of the 24th international conference on Machine learning*, pages 745–750.
- [90] Poole, B., Ozair, S., Van Den Oord, A., Alemi, A., and Tucker, G. (2019). On variational bounds of mutual information. In *International conference on machine learning*, pages 5171–5180. PMLR.

- [91] Radford, A., Kim, J. W., Hallacy, C., Ramesh, A., Goh, G., Agarwal, S., Sastry, G., Askell, A., Mishkin, P., Clark, J., et al. (2021). Learning transferable visual models from natural language supervision. In *International conference on machine learning*, pages 8748–8763. PmLR.
- [92] Radford, A., Narasimhan, K., Salimans, T., Sutskever, I., et al. (2018). Improving language understanding by generative pre-training.
- [93] Ren, A. Z., Lidard, J., Ankile, L. L., Simeonov, A., Agrawal, P., Majumdar, A., Burchfiel, B., Dai, H., and Simchowitz, M. (2025). Diffusion policy policy optimization. In *The Thirteenth International Conference on Learning Representations*.
- [94] Rummery, G. A. and Niranjan, M. (1994). *On-line Q-learning using connectionist systems*, volume 37. University of Cambridge, Department of Engineering Cambridge, UK.
- [95] Saxe, A. M., Bansal, Y., Dapello, J., Advani, M., Kolchinsky, A., Tracey, B. D., and Cox, D. D. (2018). On the information bottleneck theory of deep learning. In *International Conference on Learning Representations*.
- [96] Schulman, J., Levine, S., Abbeel, P., Jordan, M., and Moritz, P. (2015). Trust region policy optimization. In *International conference on machine learning*, pages 1889–1897. PMLR.
- [97] Schulman, J., Wolski, F., Dhariwal, P., Radford, A., and Klimov, O. (2017). Proximal policy optimization algorithms. *arXiv preprint arXiv:1707.06347*.
- [98] Schwarzer, M., Anand, A., Goel, R., Hjelm, R. D., Courville, A., and Bachman, P. (2020). Data-efficient reinforcement learning with self-predictive representations. *arXiv preprint arXiv:2007.05929*.
- [99] Sermanet, P., Lynch, C., Chebotar, Y., Hsu, J., Jang, E., Schaal, S., Levine, S., and Brain, G. (2018). Time-contrastive networks: Self-supervised learning from video. In *2018 IEEE international conference on robotics and automation (ICRA)*, pages 1134–1141. IEEE.
- [100] Sikchi, H., Zheng, Q., Zhang, A., and Niekum, S. (2024). Dual RL: Unification and new methods for reinforcement and imitation learning. In *The Twelfth International Conference on Learning Representations*.
- [101] Sohl-Dickstein, J., Weiss, E., Maheswaranathan, N., and Ganguli, S. (2015). Deep unsupervised learning using nonequilibrium thermodynamics. In *International conference on machine learning*, pages 2256–2265. pmlr.
- [102] Song, Y., Sohl-Dickstein, J., Kingma, D. P., Kumar, A., Ermon, S., and Poole, B. (2021). Score-based generative modeling through stochastic differential equations. In *International Conference on Learning Representations*.
- [103] Sutton, R. S., Barto, A. G., et al. (1998). *Reinforcement learning: An introduction*, volume 1. MIT press Cambridge.
- [104] Talvitie, E. (2014). Model regularization for stable sample rollouts. In *UAI*, pages 780–789.
- [105] Tarasov, D., Kurenkov, V., Nikulin, A., and Kolesnikov, S. (2023a). Revisiting the minimalist approach to offline reinforcement learning. *Advances in Neural Information Processing Systems*, 36:11592–11620.
- [106] Tarasov, D., Nikulin, A., Akimov, D., Kurenkov, V., and Kolesnikov, S. (2023b). Corl: Research-oriented deep offline reinforcement learning library. *Advances in Neural Information Processing Systems*, 36:30997–31020.
- [107] Tassa, Y., Doron, Y., Muldal, A., Erez, T., Li, Y., Casas, D. d. L., Budden, D., Abdolmaleki, A., Merel, J., Lefrancq, A., et al. (2018). Deepmind control suite. *arXiv preprint arXiv:1801.00690*.
- [108] Team, G., Anil, R., Borgeaud, S., Alayrac, J.-B., Yu, J., Soricut, R., Schalkwyk, J., Dai, A. M., Hauth, A., Millican, K., et al. (2023). Gemini: a family of highly capable multimodal models. *arXiv preprint arXiv:2312.11805*.

- [109] Team, O. M., Ghosh, D., Walke, H., Pertsch, K., Black, K., Mees, O., Dasari, S., Hejna, J., Kreiman, T., Xu, C., et al. (2024). Octo: An open-source generalist robot policy. *arXiv preprint arXiv:2405.12213*.
- [110] Thakoor, S., Rowland, M., Borsa, D., Dabney, W., Munos, R., and Barreto, A. (2022). Generalised policy improvement with geometric policy composition. In *International Conference on Machine Learning*, pages 21272–21307. PMLR.
- [111] Tishby, N., Pereira, F. C., and Bialek, W. (2000). The information bottleneck method. *arXiv preprint physics/0004057*.
- [112] Tomar, M., Hansen-Estruch, P., Bachman, P., Lamb, A., Langford, J., Taylor, M. E., and Levine, S. (2024). Video occupancy models. *arXiv preprint arXiv:2407.09533*.
- [113] Touati, A. and Ollivier, Y. (2021). Learning one representation to optimize all rewards. *Advances in Neural Information Processing Systems*, 34:13–23.
- [114] Touati, A., Rapin, J., and Ollivier, Y. (2023). Does zero-shot reinforcement learning exist? In *The Eleventh International Conference on Learning Representations*.
- [115] Toussaint, M. and Storkey, A. (2006). Probabilistic inference for solving discrete and continuous state markov decision processes. In *Proceedings of the 23rd international conference on Machine learning*, pages 945–952.
- [116] Touvron, H., Martin, L., Stone, K., Albert, P., Almahairi, A., Babaei, Y., Bashlykov, N., Batra, S., Bhargava, P., Bhosale, S., et al. (2023). Llama 2: Open foundation and fine-tuned chat models. *arXiv preprint arXiv:2307.09288*.
- [117] Valieva, K. and Banerjee, B. (2024). Quasimetric value functions with dense rewards. *arXiv preprint arXiv:2409.08724*.
- [118] Van Hasselt, H., Guez, A., and Silver, D. (2016). Deep reinforcement learning with double q-learning. In *Proceedings of the AAAI conference on artificial intelligence*, volume 30.
- [119] Vaswani, A., Shazeer, N., Parmar, N., Uszkoreit, J., Jones, L., Gomez, A. N., Kaiser, Ł., and Polosukhin, I. (2017). Attention is all you need. *Advances in neural information processing systems*, 30.
- [120] Walke, H. R., Black, K., Zhao, T. Z., Vuong, Q., Zheng, C., Hansen-Estruch, P., He, A. W., Myers, V., Kim, M. J., Du, M., et al. (2023). Bridgedata v2: A dataset for robot learning at scale. In *Conference on Robot Learning*, pages 1723–1736. PMLR.
- [121] Wang, Q., Xiong, J., Han, L., Liu, H., Zhang, T., et al. (2018). Exponentially weighted imitation learning for batched historical data. *Advances in Neural Information Processing Systems*, 31.
- [122] Wang, Z., Hunt, J. J., and Zhou, M. (2023). Diffusion policies as an expressive policy class for offline reinforcement learning. In *The Eleventh International Conference on Learning Representations*.
- [123] Watkins, C. J. and Dayan, P. (1992). Q-learning. *Machine learning*, 8:279–292.
- [124] Xiao, T., Radosavovic, I., Darrell, T., and Malik, J. (2022). Masked visual pre-training for motor control. *arXiv preprint arXiv:2203.06173*.
- [125] Yarats, D., Brandfonbrener, D., Liu, H., Laskin, M., Abbeel, P., Lazaric, A., and Pinto, L. (2022). Don’t change the algorithm, change the data: Exploratory data for offline reinforcement learning. In *ICLR 2022 Workshop on Generalizable Policy Learning in Physical World*.
- [126] Yu, T., Kumar, A., Chebotar, Y., Hausman, K., Finn, C., and Levine, S. (2022). How to leverage unlabeled data in offline reinforcement learning. In *International Conference on Machine Learning*, pages 25611–25635. PMLR.

- [127] Zhai, X., Mustafa, B., Kolesnikov, A., and Beyer, L. (2023). Sigmoid loss for language image pre-training. In *Proceedings of the IEEE/CVF international conference on computer vision*, pages 11975–11986.
- [128] Zhang, A., McAllister, R. T., Calandra, R., Gal, Y., and Levine, S. (2021). Learning invariant representations for reinforcement learning without reconstruction. In *International Conference on Learning Representations*.
- [129] Zheng, C., Salakhutdinov, R., and Eysenbach, B. (2024). Contrastive difference predictive coding. *The Twelfth International Conference on Learning Representations*.
- [130] Zheng, C., Tuyls, J., Peng, J., and Eysenbach, B. (2025). Can a MISL fly? analysis and ingredients for mutual information skill learning. In *The Thirteenth International Conference on Learning Representations*.
- [131] Zhou, Z., Peng, A., Li, Q., Levine, S., and Kumar, A. (2025). Efficient online reinforcement learning fine-tuning need not retain offline data. In *The Thirteenth International Conference on Learning Representations*.
- [132] Zhu, C., Wang, X., Han, T., Du, S. S., and Gupta, A. (2024). Distributional successor features enable zero-shot policy optimization. *arXiv preprint arXiv:2403.06328*.

A Preliminaries

A.1 Actor-critic framework

Prior actor-critic methods [96, 97, 36, 33, 59, 32] typically maximize the RL objective $J(\pi)$ by (1) learning an estimate Q of Q^π via the temporal difference (TD) loss (policy evaluation) and then (2) improving the policy π by selecting actions that maximizes Q (policy improvement):

$$\begin{aligned} Q^{k+1} &\leftarrow \arg \max_Q \mathbb{E}_{(s,a,r,s') \sim p^\beta(s,a,r,s'), a' \sim \pi^k(a'|s')} \left[(Q(s,a) - (r + \gamma Q^k(s',a')))^2 \right] \\ \pi^{k+1} &\leftarrow \arg \max_\pi \mathbb{E}_{s \sim p^\beta, a \sim \pi(a|s)} [Q^{k+1}(s,a)], \end{aligned}$$

where k indicates the number of updates and β is the behavioral policy representing either a replay buffer (online RL) or a fixed dataset (offline RL).

A.2 Flow matching

The goal of flow matching methods is to transform a simple noise distribution (e.g., a d -dimensional standard Gaussian) into a target distribution $p_{\mathcal{X}}$ over some space $\mathcal{X} \subset \mathbb{R}^d$ that we want to approximate. Specifically, flow matching uses a time-dependent vector field $v : [0, 1] \times \mathbb{R}^d \rightarrow \mathbb{R}^d$ to construct a time-dependent diffeomorphic flow $\phi : [0, 1] \times \mathbb{R}^d \rightarrow \mathbb{R}^d$ [63, 64] that realizes the transformation from a single noise ϵ to a generative sample \hat{x} , following the ODE

Algorithm 3 Euler method for solving the flow ODE (Eq. 10).

- 1: **Input** The vector field v and the noise ϵ . (Optional) The number of steps T with default $T = 10$.
 - 2: Initialize $t = 0$ and $x^t = \epsilon$.
 - 3: **for** each step $t = 0, 1, \dots, T - 1$ **do**
 - 4: $x^{t+1} \leftarrow x^t + v(t/T, x^t)/T$.
 - 5: **Return** $\hat{x} = x^T$.
-

$$\frac{d}{dt} \phi(t, \epsilon) = v(t, \phi(t, \epsilon)), \quad \phi(0, \epsilon) = \epsilon, \quad \phi(1, \epsilon) = \hat{x}. \quad (10)$$

We will use t to denote a time step for flow matching and sample the noise ϵ from a standard Gaussian distribution $\mathcal{N}(0, I)$ throughout our discussions.⁷ Prior work has proposed various formulations for learning the vector field [63, 17, 65, 4] and we adopt the simplest flow matching objective building upon optimal transport [65] and conditional flow matching (CFM) [63],

$$\mathcal{L}_{\text{CFM}}(v) = \mathbb{E}_{\substack{t \sim \text{UNIF}([0,1]), \\ x \sim p_{\mathcal{X}}(x), \epsilon \sim \mathcal{N}(0,I)}} [\|v(t, x^t) - (x - \epsilon)\|_2^2], \quad (11)$$

where $\text{UNIF}([0, 1])$ is the uniform distribution over the unit interval and $x^t = tx + (1 - t)\epsilon$ is a linear interpolation between the ground truth sample x and the Gaussian noise ϵ . Importantly, we can generate a sample from the vector field v by numerically solving the ODE (Eq. 10). We will use the Euler method (Alg. 3) as our ODE solver following prior practice [65, 85, 30].

B Theoretical analyses

B.1 The evidence lower bound and its connection with an information bottleneck

We first derive the evidence lower bound for optimizing the latent variable model and then show its connection with an information bottleneck. Given the unlabeled dataset D , we want to maximize the likelihood of consecutive transitions (s, a, s', a') and a future state s_f sampled from the same trajectory following the behavioral joint distribution $p^\beta(s, a, s_f, s', a') = p^\beta(s)\beta(a | s)p_\gamma^\beta(s_f | s, a)p(s' | s, a)\beta(a' | s')$. We use (s', a') to encode the intention z by the encoder $p_e(z | s, a)$ and (s, a, s_f, z) to learn the occupancy models $q_d(s_f | s, a, z)$, employing an ELBO of the likelihood of

⁷In theory, the noise can be drawn from any distribution, not necessarily limited to a Gaussian [65].

the prior data:

$$\begin{aligned}
& \mathbb{E}_{p^\beta(s, a, s_f)} [\log q_d(s_f | s, a)] \\
&= \mathbb{E}_{p^\beta(s, a, s_f, s', a')} [\log q_d(s_f | s, a)] \\
&= \mathbb{E}_{p^\beta(s, a, s_f, s', a')} [\log \mathbb{E}_{p(z)} [q_d(s_f | s, a, z)]] \\
&\stackrel{(a)}{=} \mathbb{E}_{p^\beta(s, a, s_f, s', a')} \left[\log \mathbb{E}_{p(z)} \left[q_d(s_f | s, a, z) \frac{p_e(z | s', a')}{p_e(z | s', a')} \right] \right] \\
&\stackrel{(b)}{\geq} \mathbb{E}_{p^\beta(s, a, s_f, s', a')} [\mathbb{E}_{p_e(z | s', a')} [\log q_d(s_f | s, a, z)] - D_{\text{KL}}(p_e(z | s', a') \| p(z))] \\
&\stackrel{(c)}{\geq} \mathbb{E}_{p^\beta(s, a, s_f, s', a')} [\mathbb{E}_{p_e(z | s', a')} [\log q_d(s_f | s, a, z)] - \lambda D_{\text{KL}}(p_e(z | s', a') \| p(z))] \\
&= L(p_e, q_d).
\end{aligned}$$

where in (a) we introduce the amortized variational encoder $p_e(z | s', a')$, in (b) we apply the Jensen's inequality [24], and in (c) we introduce a coefficient λ to control the strength of the KL divergence regularization as in Higgins et al. [45]. This ELBO can also be cast as a variational lower bound on an information bottleneck with the chain of random variables $(S', A') \rightarrow Z \rightarrow (S, A, S_f)$ [111, 5, 95]:

$$\begin{aligned}
& I^\beta(S, A, S_f; Z) - \lambda I^\beta(S', A'; Z) \\
&\stackrel{(a)}{=} I^\beta(S, A, S_f; Z) - \lambda \mathbb{E}_{p^\beta(s', a')} [D_{\text{KL}}(p_e(z | s', a') \| p_e(z))] \\
&\stackrel{(b)}{\geq} I^\beta(S, A, S_f; Z) - \lambda \mathbb{E}_{p^\beta(s', a')} [D_{\text{KL}}(p_e(z | s', a') \| p(z))] \\
&\stackrel{(c)}{\geq} \mathbb{E}_{p^\beta(s, a, s_f, s', a')}_{p_e(z | s', a')} [\log q_d(s, a, s_f | z)] - \lambda \mathbb{E}_{p^\beta(s', a')} [D_{\text{KL}}(p_e(z | s', a') \| p(z))] + H^\beta(S, A, S_f) \\
&\stackrel{(d)}{\geq} \mathbb{E}_{p^\beta(s, a, s_f, s', a')}_{p_e(z | s', a')} [\log q_d(s_f | s, a, z)] - \lambda \mathbb{E}_{p^\beta(s', a')} [D_{\text{KL}}(p_e(z | s', a') \| p(z))] + \text{const} \\
&= L(p_e, q_d) + \text{const},
\end{aligned}$$

where in (a) we use the definition of $I^\beta(S', A'; Z)$ and $p_e(z)$ is the marginal distribution of latent intentions z defined as $p_e(z) = \int p^\beta(s', a') p_e(z | s', a') ds' da'$, in (b) we apply the non-negative property of the KL divergence $D_{\text{KL}}(p_e(z) \| p(z))$, in (c) we apply the standard variation lower bound of the mutual information [7, 90] to incorporate the decoder (occupancy models) $q_d(s, a, s_f | z)$, and in (d) we choose the variational decoder to satisfy $\log q_d(s, a, s_f | z) = \log p^\beta(s, a) + \log q_d(s_f | s, a, z)$ and consider the entropy $H^\beta(S, A, S_f)$ as a constant.

B.2 Intutions and discussions about the implicit generalized policy improvement

The intuition for the expectile distillation loss (Eq. 8) is that the scalar Q function $Q(\cdot, \cdot)$ is a *one-step* summary of the average reward at future states sampled from the flow occupancy models, while the expectile loss serves as a "softmax" operator over the entire latent intention space. Theoretically, this expectile loss is guaranteed to converge to the maximum over $p(z)$ under mild assumptions (See Sec. 4.4 in Kostrikov et al. [58] for details). Therefore, given an infinite amount of samples ($N \rightarrow \infty$) and an expectile $\mu \rightarrow 1$, the Q converges to the greedy value functions:

$$Q^*(s, a) = \max_{z \sim p(z)} \frac{1}{(1 - \gamma)} \mathbb{E}_{q_d(s_f | s, a, z)} [r(s_f)].$$

If we further assume that the flow occupancy models are optimal, i.e., $q_d^*(s_f | s, a, z) = p^\beta(s_f | s, a, z)$, then the optimal Q corresponds to a greedy value functions under the behavioral policy β :

$$Q^*(s, a) = \max_{z \sim p(z)} Q^\beta(s, a, z).$$

Unlike Q-learning which converges to the optimal Q-function sequentially [123, 103], the implicit GPI proposes a new policy that is strictly no worse than the set of policies that correspond to each $\hat{Q}(\cdot, \cdot, z)$ in parallel (See Sec. 4.1 in Barreto et al. [9] for further discussions). Unlike one-step policy improvement [121, 14, 89, 88], implicit GPI is able to converge to the optimal policy for a downstream task, assuming that the task-specific intention has been captured during pre-training.

B.3 One-step policy improvement with flow occupancy models

The FOM + one-step PI variant performs one-step policy improvement using a flow occupancy model $q_d(s_f | s, a)$ that is *not* conditioned on latent intentions. This flow occupancy model captures the discounted state occupancy measure of the (average) behavioral policy. After training the flow occupancy model, FOM + one-step PI fits a Q function and extracts a behavioral-regularized policy:

$$Q \leftarrow \arg \min_Q \frac{1}{1 - \gamma} \mathbb{E}_{(s,a) \sim p^{\tilde{\beta}}(s,a), s_f \sim q_d(s_f | s,a)} [(Q(s, a) - r(s_f))^2],$$

$$\pi \leftarrow \arg \max_{\pi} \mathbb{E}_{(s,a) \sim p^{\tilde{\beta}}(s,a), a^{\pi} \sim \pi(a^{\pi} | s)} [Q(s, a^{\pi}) + \alpha \log \pi(a | s)].$$

Intuitively, the first objective fits the behavioral Q function based on the dual definition (Eq. 3), and the second objective trains a policy to maximize this behavioral Q function, invoking one-step policy improvement. While this simple objective sometimes achieves strong performance on some benchmark tasks [14, 28], it does not guarantee convergence to the optimal policy due to the use of a behavioral value function.

C Experimental details

We implement InFOM and all baselines in the same codebase using JAX [13]. Our implementations build on top of OGBench’s and FQL’s implementations [81, 85]. All the experiments were run on a single NVIDIA A6000 GPU and can be finished in 4 hours for state-based tasks and 12 hours for image-based tasks. We provide open-source implementations of InFOM and all baselines at <https://github.com/chongyi-zheng/infom>.

C.1 Tasks and datasets

Our experiments use a suite of 36 state-based and 4 image-based control tasks taken from ExORL benchmarks [125] and OGBench task suite [81] (Fig. 2).

ExORL. We use 16 state-based tasks from the ExORL [125] benchmarks based on the DeepMind Control Suite [107]. These tasks involve controlling four robots (cheetah, walker, quadruped, and jaco) to achieve different locomotion behaviors. For each domain, the specific tasks are: cheetah {run, run backward, walk, walk backward}, walker {walk, run, stand, flip}, quadruped {run, jump, stand, walk}, jaco {reach top left, reach top right, reach bottom left, reach bottom right}. For all tasks in cheetah, walker, and quadruped, both the episode length and the maximum return are 1000. For all tasks in jaco, both the episode length and the maximum return are 250.

Following the prior work [114, 84, 55], we will use 5M unlabeled transitions collected by some exploration methods (e.g., RND [16]) for pre-training, and another 500K reward-labeled transitions collected by the same exploratory policy for fine-tuning. Fine-tuning datasets are labeled with task-specific dense rewards [125].

OGBench. We use 20 state-based manipulation tasks from four domains (cube single, cube double, scene, and puzzle 4x4) in the OGBench task suite [81], where the goal is to control a simulated robot arm to rearrange various objects. For each domain, the specific tasks are: cube single {task 1 (pick and place cube to left), task 2 (pick and place cube to front), task 3 (pick and place cube to back), task 4 (pick and place cube diagonally), task 5 (pick and place cube off-diagonally)}, cube double {task 1 (pick and place one cube), task 2 (pick and place two cubes to right), task 3 (pick and place two cubes off-diagonally), task 4 (swap cubes), task 5 (stack cubes)}, scene {task 1 (open drawer and window), task 2 (close and lock drawer and window), task 3 (open drawer, close window, and pick and place cube to right), task 4 (put cube in drawer), task 5 (fetch cube from drawer and close window)}, puzzle 4x4 {task 1 (all red to all blue), task 2 (all blue to central red), task 3 (two blue to mix), task 4 (central red to all red), task 5 (mix to all red)}. Note that some of these tasks, e.g., cube double task 5 (stack cubes) and scene task 4 (put cube in drawer), involve interacting with the environment in a specific order and thus require long-horizon temporal reasoning. For all tasks in cube single, cube double, and scene, the maximum episode length is 400. For all tasks in puzzle 4x4, the maximum episode length is 800.

We also use 4 image-based tasks in the OGBench task suite. Specifically, we consider `visual cube single task 1`, `visual cube double task 1`, `visual scene task 1`, and `visual puzzle 4x4 task 1` from each domain respectively. The observations are $64 \times 64 \times 3$ RGB images. These tasks are challenging because the agent needs to reason from pixels directly. All the manipulation tasks from OGBench are originally designed for evaluating goal-conditioned RL algorithms [81].

For both state-based and image-based tasks from OGBench, we will use 1M unlabeled transitions collected by a non-Markovian expert policy with temporally correlated noise (the play datasets) for pre-training, and another 500K reward-labeled transitions collected by the same noisy expert policy for fine-tuning. Unlike the ExORL benchmarks, the fine-tuning datasets for OGBench tasks are relabeled with *semi-sparse* rewards [85], providing less supervision for the algorithm.

C.2 Baselines

We compare InFOM with eight baselines across five categories of prior methods focusing on different strategies for pre-training and fine-tuning in RL. First, implicit Q-Learning (IQL) [58] and revisited behavior-regularized actor-critic (ReBRAC) [105] are state-of-the-art offline RL algorithms based on the standard actor-critic framework (Appendix A.1). Second, we compare to a variant of ReBRAC learning on top of representations pre-trained on the unlabeled datasets. We choose an off-the-shelf self-supervised learning objective in vision tasks called self-distillation with no labels (DINO) [18] as our representation learning loss and name the resulting baseline DINO + ReBRAC. Third, our next baseline, model-based policy optimization (MBPO) [50], pre-trains a one-step model to predict transitions in the environment, similar to the next token prediction in language models [92]. The one-step model is then used to augment the datasets for downstream policy optimization. We will again use ReBRAC to extract the policy (MBPO + ReBRAC). Fourth, we also include comparisons against the InfoNCE variant of contrastive RL [26] and temporal difference InfoNCE [129], which pre-train the discounted state occupancy measure using monte carlo or temporal difference contrastive losses. While our method fits generative occupancy models, These two approaches predict the ratio of occupancy measures over some marginal densities serving as the discriminative counterparts. After pre-training the ratio predictors, importance sampling is required to recover the Q function (CRL + IS & TD InfoNCE + IS) [70, 129], enabling policy maximization. Fifth, our final set of baselines are prior unsupervised RL methods that pre-train a set of latent intentions and intention-conditioned policies using forward-backward representations [113] or a Hilbert space [84]. Given a downstream task, these methods first infer the corresponding intention in a zero-shot manner and then fine-tune the policy using offline RL [55], differing from the implicit GPI as in our method. We will use IQL as the fine-tuning algorithm and call the resulting methods FB + IQL and HILP + IQL. For image-based tasks, we selectively compare to four baselines ReBRAC, CRL + IS, DINO + ReBRAC, and FB + IQL.

C.3 Evaluation protocols

We compare the performance of InFOM against the eight baselines (Sec. 5.1) after first pre-training each method for 1M gradient steps (250K gradient steps for image-based tasks) and then fine-tuning for 500K gradient steps (100K gradient steps for image-based tasks). We measure the episode return for tasks from ExORL benchmarks and the success rate for tasks from the OGBench task suite. For OGBench tasks, the algorithms still use the semi-sparse reward instead of the success rate for training. Following prior practice [85, 106], We do *not* report the best performance during fine-tuning and report the evaluation results averaged over 400K, 450K, and 500K gradient steps instead. For image-based tasks, we report the evaluation results averaged over 50K, 75K, and 100K gradient steps during fine-tuning. For evaluating the performance of different methods throughout the entire fine-tuning process, we defer the details into specific figures (e.g., Fig. 6 & 4).

C.4 Implementations and hyperparameters

In this section, we discuss the implementation details and hyperparameters for InFOM and the eight baselines. Whenever possible, we use the same set of hyperparameters for all methods (Table 1) across all tasks, including learning rate, network architecture, batch size, image encoder, etc. Of particular note is that we use asynchronous policy training [131], where we update the policy 4 times less frequently than other models during fine-tuning. For specific hyperparameters of each method,

Table 1: Common hyperparameters for our method and the baselines.

Hyperparameter	Value
learning rate	3×10^{-4}
optimizer	Adam [56]
pre-training gradient steps	1×10^6 for state-based tasks, 2.5×10^5 for image-based tasks
fine-tuning gradient steps	5×10^5 for state-based tasks, 1×10^5 for image-based tasks
batch size	256
MLP hidden layer sizes	(512, 512, 512, 512)
MLP activation function	GELU [44]
discount factor γ	0.99
target network update coefficient	5×10^{-3}
double Q aggregation	min
policy update frequency in fine-tuning	1/4
image encoder	small IMPALA encoder [25, 85]
image augmentation method	random cropping
image augmentation probability	1.0 for DINO + ReBRAC, 0.5 for all other methods
image frame stack	3

Table 2: **Hyperparameters for InFOM.** See Appendix C.4 for descriptions of each hyperparameter.

Hyperparameter	Value
latent intention dimension d	See Table 3
number of steps for the Euler method T	10
number of future states N	16
normalize the Q loss term in $\mathcal{L}(\pi)$ (Eq. 9)	No
expectile μ	See Table 3
KL divergence regularization coefficient λ	See Table 3
behavioral cloning regularization coefficient α	See Table 3

we tune them on the following tasks from each domain and use one set of hyperparameters for every task in that domain. For image-based tasks, we tune hyperparameters for each task individually.

- cheetah: cheetah run
- walker: walker walk
- quadruped: quadruped jump
- jaco: jaco reach top left
- cube single: cube single task 2
- cube double: cube double task 2
- scene: scene task 2
- puzzle 4x4: puzzle 4x4 task 4

InFOM. InFOM consists of two main components for pre-training: the intention encoder and the flow occupancy models. First, we use a Gaussian distribution conditioned on the next state-action pair as the intention encoding distribution. Following prior work [57, 5], we model the intention encoder as a multilayer perceptron (MLP) that takes the next state-action pair (s', a') as input and outputs two heads representing the mean and the (log) standard deviation of the Gaussian. We apply layer normalization to the intention encoder to stabilize optimization. We use the reparameterization trick [57] to backpropagate the gradients from the flow-matching loss and the KL divergence regularization (Eq. 6) into the intention encoder. Our initial experiments suggest that the dimension of the latent intention space d is an important hyperparameter and we sweep over $\{64, 128, 256, 512\}$ and find that $d = 512$ is sufficient for most ExORL tasks and $d = 128$ is generally good enough for all OGBench tasks. For the coefficient of the KL divergence regularization λ , we sweep over $\{2.0, 1.0, 0.2, 0.1, 0.05, 0.025, 0.01, 0.005\}$ to find the best λ for each domain.

Table 3: **Domain-specific hyperparameters for our method and the baselines.** We individually tune these hyperparameters for each domain and use the same set of hyperparameters for tasks in the same domain. See Appendix C.4 for tasks used to tune these hyperparameters and descriptions of each hyperparameter. “-” indicates that the hyperparameter does not exist.

Domain or Task	d	InFOM (Ours)			IQL		ReBRAC		DINO + ReBRAC		MBPO + ReBRAC		CRL + IS	TD InfoNCE + IS	FB + IQL		HILP + IQL
		μ	λ	α	α	α	α_{actor}	α_{critic}	β_{student}	$N_{\text{imaginary}}$	$H_{\text{imaginary}}$	α	α	α	α_{repr}	α_{AWR}	α
cheetah	128	0.9	0.05	0.3	1	0.1	0.1	0.1	0.1	128	1	0.03	0.003	1	1	1	1
walker	512	0.9	0.1	0.3	1	10	0.1	0.1	0.1	128	1	0.03	0.03	1	10	10	10
quadruped	512	0.9	0.005	0.3	10	1	1	0.1	0.1	128	1	0.03	0.03	10	1	10	10
jaco	512	0.9	0.2	0.1	0.1	0.1	0.1	0.1	0.1	128	1	0.003	0.03	1	1	1	1
cube single	512	0.95	0.05	30	1	1	1	0.04	0.04	256	2	30	30	10	1	1	1
cube double	128	0.9	0.025	30	1	1	1	0.04	0.04	256	2	30	30	1	10	1	1
scene	128	0.99	0.2	300	1	1	1	0.1	0.1	256	2	3	3	10	10	1	1
puzzle 4x4	128	0.95	0.1	300	10	0.1	0.1	0.1	0.1	256	2	3	3	10	10	1	1
visual cube single task 1	512	0.95	0.025	30	-	1	0	0.1	0.1	-	-	30	-	10	1	-	-
visual cube double task 1	128	0.9	0.01	30	-	0.1	0	0.1	0.1	-	-	30	-	10	1	-	-
visual scene task 1	128	0.99	0.1	300	-	0.1	0.01	0.1	0.1	-	-	3	-	10	10	-	-
visual puzzle 4x4 task 1	128	0.95	0.1	300	-	0.1	0.01	0.1	0.1	-	-	3	-	10	10	-	-

Second, we use flow-matching vector fields to model the flow occupancy models. The vector field is an MLP that takes in a noisy future state s_f^t , a state-action pair (s, a) , and a latent intention z , and outputs the vector field with the same dimension as the state. We apply layer normalization to the vector field to stabilize optimization. As mentioned in Sec. 3, we use flow-matching objectives based on optimal transport (linear path) and sample the time step t from the uniform distribution over the unit interval. Following prior work [85], we use a fixed $T = 10$ steps (step size = 0.1) for the Euler method and do not apply a sinusoidal embedding for the time. To make a fair comparison with other baselines, we also pre-train a behavioral cloning policy that serves as initialization for fine-tuning.

For fine-tuning, InFOM learns three components: the reward predictor, the critic, and the policy, while fine-tunes the intention encoder and the flow occupancy models. The reward predictor is an MLP that predicts the scalar reward of a state trained using mean squared error. We apply layer normalization to the reward predictor to stabilize learning. The critic is an MLP that predicts double Q values [118, 33] of a state-action pair, without conditioned on the latent intention. We apply layer normalization to the critic to stabilize learning. We train the critic using the expectile distillation loss (Eq. 8) and sweep the expectile over $\{0.9, 0.95, 0.99\}$ to find the best μ for each domain. We use $N = 16$ future states sampled from the flow occupancy models to compute the average reward, which we find to be sufficient. We use the minimum of the double Q predictions to prevent overestimation. The policy is an MLP that outputs a Gaussian distribution with a unit standard deviation. In our initial experiments, we find that the behavioral cloning coefficient α in Eq. 9 is important and we sweep over $\{300, 30, 3, 0.3\}$ to find the best α for each domain. Following prior practice [85], we do not normalize the Q loss term in the actor loss $\mathcal{L}(\pi)$ (Eq. 9) as in Fujimoto and Gu [32]. Other choices of the policy network include the diffusion model [93, 122] and the flow-matching model [85], and we leave investigating these policy networks to future work.

For image-based tasks, following prior work [85], we use a smaller variant of the IMPALA encoder [25] and apply random cropping augmentation with a probability of 0.5. We also apply frame stacking with three images. Table 2 and Table 3 summarize the hyperparameters for InFOM.

IQL and ReBRAC. We reuse the IQL [58] implementation and the ReBRAC [105] implementation from Park et al. [85]. Since learning a critic requires reward-labeled datasets or relabeling rewards for unlabeled datasets [126], we simply pre-train a behavioral cloning policy. During the fine-tuning, we use the behavioral cloning policy as initialization and trains a critic from scratch using the TD error [58, 32, 105]. Following prior work [85], we use the same expectile value 0.9 for IQL on all tasks, and sweep over $\{100, 10, 1, 0.1, 0.01\}$ to find the best AWR inverse temperature α for each domain. For ReBRAC, we tune the behavioral cloning (BC) regularization coefficients for the actor and the critic separately. We use the range $\{100, 10, 1, 0.1\}$ to search for the best actor BC coefficient α_{actor} and use the range $\{100, 10, 1, 0.1, 0\}$ to search for the best critic BC coefficient α_{critic} . We use the default values for other hyperparameters following the implementation from Park et al. [85]. See Table 3 for domain-specific hyperparameters.

DINO + ReBRAC. We implement DINO on top of ReBRAC. DINO [18] learns a state encoder using two augmentations of the same state. For state-based tasks, the state encoder is an MLP that outputs representations. We apply two clipped Gaussian noises centered at zero to the same state to obtain those augmentations. The standard deviation of the Gaussian noise is set to 0.2 and we clip the

noises into $[-0.2, 0.2]$ on all domains. For image-based tasks, the state encoder is the small IMPALA encoder also outputting representations. We apply two different random cropings to the same image observation to obtain those augmentations. We sweep over $\{0.01, 0.04, 0.1, 0.4\}$ for the temperature for student representations κ_{student} and use a fixed temperature 0.04 for teacher representations on all domains. We use a representation space with 512 dimensions. We update the target representation centroid with a fixed ratio 0.1. During pre-training, we learn the DINO representations along with a behavioral cloning policy. During fine-tuning, we learn the actor and the critic using ReBRAC on top of DINO representations, while continuing to fine-tune those DINO representations. We use the same BC coefficients α_{actor} and α_{critic} as in ReBRAC. For image-based tasks, we apply random cropping to the same image twice with a probability of 1.0 and use those two augmentations to compute the teacher and the student representations. See Table 3 for domain-specific temperatures for student representations.

MBPO + ReBRAC. We implement MBPO [50] on top of ReBRAC and only consider this baseline for state-based tasks. MBPO learns a one-step transition MLP to predict the residual between the next state s' and the current state s conditioned on the current state-action pair (s, a) . We pre-train the one-step model with a behavioral cloning policy. During fine-tuning, we use the model with a learned reward predictor to collect imaginary rollouts. We *only* use these imaginary rollouts to learn the actor and the critic. We sweep over $\{64, 128, 256\}$ for the number of imaginary rollouts to collect for each gradient step $N_{\text{imaginary}}$ and sweep over $\{1, 2, 4\}$ for the number of steps in each rollout $H_{\text{imaginary}}$. We use the same BC coefficient as in ReBRAC. See Table 3 for the domain-specific number of imaginary rollouts and number of steps in each rollout.

CRL + IS and TD InfoNCE + IS. We mostly reuse the CRL [28] implementation based on the InfoNCE loss from Park et al. [81] and adapt it to our setting by adding the important sampling component. We implement TD InfoNCE by adapting the official implementations [129]. For both methods, we pre-train the classifiers that predict the ratio between the occupancy measures and the marginal densities over future states with a behavioral cloning policy. We use the SARSA variant of TD InfoNCE during pre-training. After pre-training the classifiers, we learn a reward predictor and apply importance sampling weights predicted by the classifiers to a set of future states sampled from the fine-tuning datasets to estimate Q . This Q estimation then drives policy optimization. We use a single future state from the fine-tuning dataset to construct the importance sampling estimation, which is sufficient. We use 512 dimensional contrastive representations. We sweep over $\{300, 30, 3, 0.3, 0.03\}$ for the BC coefficient α (Table 3).

FB + IQL and HILP + IQL. We implement FB [113] and HILP [84] by adapting the FB implementation from Jeon et al. [53] and the HILP implementation from Kim et al. [55]. During pre-training, for FB, we pre-train the forward-backward representations and the intention-conditioned policies in an actor-critic manner. We use a coefficient 1 for the orthonormality regularization of the backward representations. We use 512 dimensional forward-backward representations. We sample the latent intentions for pre-training from either a standard Gaussian distribution (with probability 0.5) or the backward representations for a batch of states (with probability 0.5), normalizing those latent intentions to length $\sqrt{512}$. We sweep over $\{100, 10, 1, 0.1\}$ for the BC coefficient α_{repr} . For HILP, we pre-train the Hilbert representations ϕ and Hilbert foundation policies using an actor-critic framework as well. We use implicit value learning to learn the Hilbert representations following implementations from Park et al. [82, 81]. We set the expectile to 0.9 for all domains. We sweep over $\{100, 10, 1, 0.1\}$ to find the best AWR inverse temperature α . We also use 512 dimensional Hilbert representation space. To construct the intrinsic rewards, we first sample the latent intention z from a standard Gaussian, normalizing them to length $\sqrt{512}$, and then use the representation of the next state $\phi(s')$ and the representation of the current state $\phi(s)$ to compute the intrinsic reward $(\phi(s') - \phi(s))^T z$.

During fine-tuning, we first infer a task-specific backward representation or a Hilbert representation using a small amount of transitions (10K) from the fine-tuning datasets, and then invoke IQL to learn the critic and the actor using downstream rewards conditioned on the inferred representations. For FB, we sweep over $\{100, 10, 1, 0.1\}$ for the AWR inverse temperature α_{AWR} for IQL. For HILP, we reuse the same AWR inverse temperature in representation learning for IQL. See Table 3 for domain-specific BC coefficients and AWR inverse temperatures.

Table 4: **Evaluation on ExORL and OGBench benchmarks.** Following OGBench [81], we bold values at and above 95% of the best performance for each task.

Task	InFOM (Ours)	IQL	ReBRAC	DINO + ReBRAC	MBPO + ReBRAC	CRL + IS	TD InfoNCE + IS	FB + IQL	HILP + IQL
cheetah run	97.6 ± 7.8	80.0 ± 8.4	97.2 ± 12.9	87.2 ± 8.6	104.7 ± 2.4	73.3 ± 6.7	68.2 ± 8.9	83.3 ± 10.9	90.3 ± 1.9
cheetah run backward	104.7 ± 7.3	77.0 ± 12.6	84.9 ± 3.7	67.1 ± 6.4	87.0 ± 4.8	74.7 ± 8.1	74.3 ± 17.1	67.3 ± 7.0	64.4 ± 6.4
cheetah walk	254.8 ± 158.6	357.9 ± 16.4	443.4 ± 15.3	383.5 ± 10.3	447.4 ± 12.7	327.4 ± 38.7	336.7 ± 22.1	346.5 ± 24.3	366.8 ± 6.9
cheetah walk backward	251.8 ± 116.9	303.7 ± 12.6	403.0 ± 16.1	318.4 ± 23.0	398.6 ± 16.0	330.2 ± 8.5	326.3 ± 45.1	298.0 ± 22.8	318.1 ± 11.4
walker walk	467.3 ± 82.1	208.6 ± 3.7	208.1 ± 5.8	228.0 ± 3.7	327.6 ± 4.5	213.3 ± 7.8	212.2 ± 13.2	225.3 ± 6.7	225.4 ± 3.7
walker run	116.3 ± 15.3	92.4 ± 0.6	97.8 ± 1.2	98.5 ± 1.0	107.6 ± 1.2	91.5 ± 3.2	91.0 ± 3.7	97.4 ± 1.2	97.4 ± 2.2
walker stand	581.2 ± 72.1	409.1 ± 2.3	460.6 ± 1.1	453.0 ± 3.1	458.1 ± 2.5	409.0 ± 7.5	397.2 ± 6.0	446.8 ± 7.1	443.3 ± 3.8
walker flip	358.8 ± 10.3	260.3 ± 2.8	344.6 ± 2.7	320.3 ± 4.3	341.8 ± 3.7	255.0 ± 8.0	231.6 ± 6.9	287.0 ± 3.1	280.7 ± 5.4
quadruped run	341.8 ± 41.2	358.0 ± 6.2	343.0 ± 2.6	344.7 ± 2.9	395.1 ± 2.6	323.4 ± 2.9	222.1 ± 39.7	367.0 ± 3.8	371.1 ± 11.5
quadruped jump	626.0 ± 6.8	628.5 ± 7.8	605.2 ± 7.8	573.0 ± 9.6	666.9 ± 3.4	576.7 ± 13.7	421.4 ± 33.4	639.4 ± 8.9	626.5 ± 14.5
quadruped stand	718.3 ± 18.7	714.2 ± 9.8	688.6 ± 5.0	663.2 ± 8.3	703.7 ± 3.6	653.1 ± 8.4	457.1 ± 47.7	728.9 ± 11.5	715.6 ± 13.9
quadruped walk	360.7 ± 7.9	375.1 ± 3.7	343.5 ± 7.1	391.4 ± 7.2	390.0 ± 5.7	309.6 ± 9.6	243.1 ± 29.2	388.9 ± 7.0	393.4 ± 3.4
jaco reach top left	742.5 ± 43.7	74.7 ± 19.6	59.0 ± 4.9	17.5 ± 3.8	60.1 ± 6.2	29.1 ± 4.7	31.5 ± 3.0	25.0 ± 11.4	40.4 ± 11.5
jaco reach top right	687.5 ± 46.7	40.6 ± 14.0	38.0 ± 13.1	11.0 ± 4.1	52.5 ± 10.8	21.4 ± 6.5	25.5 ± 10.3	16.2 ± 3.2	25.1 ± 9.6
jaco reach bottom left	746.7 ± 12.6	77.1 ± 12.5	44.5 ± 4.0	13.7 ± 2.8	43.4 ± 4.6	19.8 ± 8.8	26.6 ± 5.9	19.8 ± 4.0	27.8 ± 4.6
jaco reach bottom right	733.0 ± 19.6	78.7 ± 19.1	41.4 ± 5.0	8.3 ± 2.8	34.0 ± 6.0	19.6 ± 2.0	25.4 ± 5.7	12.4 ± 2.7	24.7 ± 3.9
cube single task 1	92.5 ± 4.0	53.0 ± 8.7	67.3 ± 14.2	1.8 ± 1.0	77.8 ± 11.7	10.1 ± 2.7	13.8 ± 3.8	17.7 ± 8.8	32.9 ± 9.2
cube single task 2	78.4 ± 12.3	51.7 ± 15.1	93.7 ± 3.5	1.2 ± 0.6	94.2 ± 2.0	3.7 ± 2.8	8.5 ± 5.6	16.7 ± 8.6	26.5 ± 15.4
cube single task 3	56.4 ± 36.9	41.5 ± 5.3	94.8 ± 0.8	1.5 ± 1.4	93.1 ± 4.7	12.5 ± 3.2	11.7 ± 7.4	16.0 ± 12.2	35.5 ± 14.7
cube single task 4	91.5 ± 14.2	42.2 ± 8.3	89.5 ± 3.6	0.5 ± 1.0	88.7 ± 4.7	1.7 ± 1.7	3.3 ± 3.0	18.7 ± 9.9	36.4 ± 14.9
cube single task 5	70.0 ± 39.1	33.7 ± 12.9	83.3 ± 6.8	0.5 ± 0.6	87.8 ± 2.7	4.3 ± 2.2	4.0 ± 3.2	14.2 ± 12.0	18.5 ± 5.6
cube double task 1	29.3 ± 10.5	17.8 ± 9.6	2.2 ± 1.7	0.0 ± 0.0	2.7 ± 1.1	4.1 ± 1.9	6.7 ± 2.7	0.2 ± 0.3	0.7 ± 1.1
cube double task 2	12.5 ± 10.7	1.3 ± 1.2	0.0 ± 0.0	0.0 ± 0.0	0.0 ± 0.0	0.0 ± 0.0	0.0 ± 0.0	0.0 ± 0.0	0.0 ± 0.0
cube double task 3	11.6 ± 8.3	0.3 ± 0.4	0.0 ± 0.0	0.0 ± 0.0	0.0 ± 0.0	0.0 ± 0.0	0.0 ± 0.0	0.0 ± 0.0	0.0 ± 0.0
cube double task 4	0.3 ± 0.4	0.0 ± 0.0	0.0 ± 0.0	0.0 ± 0.0	0.0 ± 0.0	0.0 ± 0.0	0.0 ± 0.0	0.0 ± 0.0	0.0 ± 0.0
cube double task 5	2.8 ± 4.6	1.5 ± 1.0	0.0 ± 0.0	0.0 ± 0.0	0.0 ± 0.0	0.3 ± 0.7	0.2 ± 0.3	0.0 ± 0.0	0.0 ± 0.0
scene task 1	97.8 ± 1.0	66.5 ± 13.1	47.7 ± 7.2	26.7 ± 4.3	35.3 ± 7.7	17.5 ± 5.1	21.0 ± 4.3	12.3 ± 11.3	8.8 ± 3.0
scene task 2	15.6 ± 3.4	2.5 ± 1.5	7.8 ± 4.9	1.3 ± 0.0	5.6 ± 5.6	2.3 ± 0.7	1.7 ± 1.3	1.5 ± 1.8	1.2 ± 1.7
scene task 3	43.5 ± 2.8	0.7 ± 0.5	1.7 ± 1.1	0.2 ± 0.3	2.4 ± 0.8	0.8 ± 0.3	0.5 ± 1.0	0.0 ± 0.0	0.0 ± 0.0
scene task 4	1.0 ± 0.7	0.2 ± 0.3	2.8 ± 0.8	0.2 ± 0.3	2.0 ± 1.3	1.2 ± 1.4	0.7 ± 1.3	0.2 ± 0.3	0.0 ± 0.0
scene task 5	0.3 ± 0.4	0.0 ± 0.0	0.0 ± 0.0	0.0 ± 0.0	0.0 ± 0.0	0.3 ± 0.1	0.0 ± 0.0	0.0 ± 0.0	0.0 ± 0.0
puzzle 4x4 task 1	24.2 ± 14.4	2.3 ± 2.3	12.8 ± 3.1	0.3 ± 0.7	16.9 ± 1.4	0.0 ± 0.0	0.0 ± 0.0	0.2 ± 0.3	0.3 ± 0.6
puzzle 4x4 task 2	14.5 ± 9.4	0.5 ± 0.6	0.5 ± 0.6	0.0 ± 0.0	0.2 ± 0.4	0.3 ± 0.4	0.0 ± 0.0	0.2 ± 0.3	0.4 ± 0.6
puzzle 4x4 task 3	26.3 ± 13.4	1.0 ± 0.9	5.0 ± 2.7	0.0 ± 0.0	5.1 ± 2.8	0.3 ± 0.4	0.0 ± 0.0	0.2 ± 0.3	0.1 ± 0.3
puzzle 4x4 task 4	12.0 ± 7.1	0.3 ± 0.7	0.8 ± 0.8	0.0 ± 0.0	0.4 ± 0.4	0.0 ± 0.0	0.0 ± 0.0	0.2 ± 0.3	0.1 ± 0.3
puzzle 4x4 task 5	12.3 ± 6.2	0.7 ± 0.8	0.0 ± 0.0	0.0 ± 0.0	0.0 ± 0.0	0.5 ± 0.6	0.0 ± 0.0	0.0 ± 0.0	0.1 ± 0.3
visual cube single task 1	52.1 ± 20.8	-	10.6 ± 7.2	15.3 ± 14.6	-	12.0 ± 5.6	-	31.0 ± 15.0	-
visual cube double task 1	11.2 ± 9.2	-	0.0 ± 1.5	5.0 ± 2.0	-	5.0 ± 3.6	-	1.3 ± 1.5	-
visual scene task 1	72.4 ± 17.7	-	32.0 ± 13.0	26.0 ± 17.2	-	9.0 ± 6.6	-	74.7 ± 22.2	-
visual puzzle 4x4 task 1	6.0 ± 3.2	-	0.0 ± 0.0	0.0 ± 0.0	-	0.0 ± 0.0	-	0.0 ± 0.0	-

D Hyperparameter ablations

We conduct additional ablation experiments on walker flip, quadruped jump, cube double task 1, and scene task 1 to study the effect of some key hyperparameters in InFOM (Table 2). Following the same evaluation protocols as in Appendix C.3, we report means and standard deviations across eight random seeds after fine-tuning each variant.

As shown in Fig. 7a, our algorithm is sensitive to the latent intention dimension d . Additionally, effects of the number of steps for the Euler method T (Fig. 7b) and the number of future states N (Fig. 7c) saturate after increasing both of them to a certain threshold ($T = 10$ and $N = 16$), suggesting the usage of fixed values for all tasks.

Results in Fig. 7d, Fig. 7e, and Fig. 7f suggest that the expectile μ can affect the performance on ExORL tasks, while having minor effects on OGBench tasks. Importantly, the KL divergence regularization coefficient λ and the behavioral cloning regularization coefficient α are crucial hyperparameters for InFOM, where domain-specific hyperparameter tuning is required. As discussed in Appendix C.4, we generally select one task from each domain to sweep hyperparameters and then use one set of hyperparameters for every task in that domain.

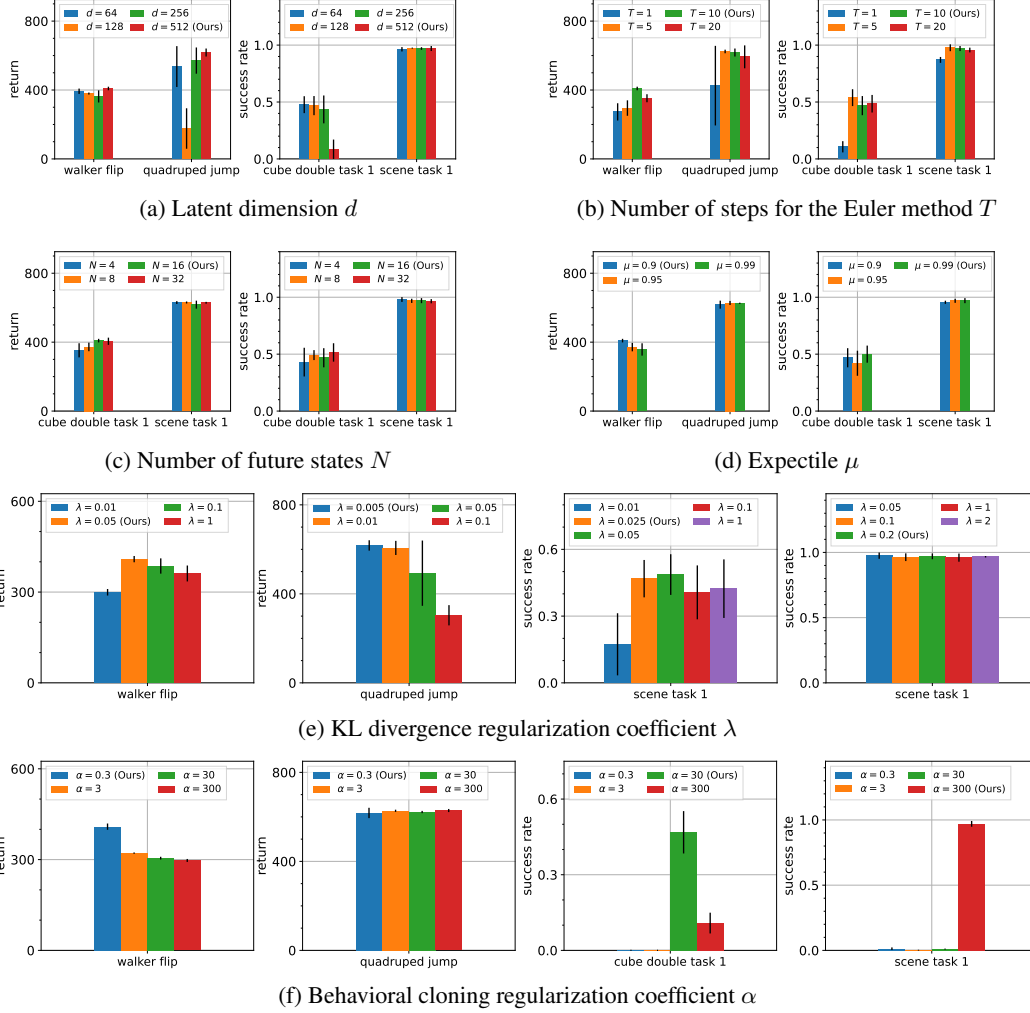


Figure 7: **Hyperparameter ablations.** We conduct ablations to study the effect of key hyperparameters of InFOM as listed in Table 2 on walker flip, quadruped jump, cube double task 1, and scene task 1.